2024

# EXPLORING THE EFFECT OF CASTING SOLUTION COMPOSITION, ADDITIVES, AND CASTING CONDITIONS ON THE MORPHOLOGY AND SEPARATION PERFORMANCE OF PVDF MEMBRANES

Rachel Kaplan
*University of Kentucky*, rlka225@g.uky.edu
Author ORCID Identifier:
https://orcid.org/0009-0007-4959-163X
Digital Object Identifier: https://doi.org/10.13023/etd.2024.354

STUDENT AGREEMENT:

I represent that my thesis or dissertation and abstract are my original work. Proper attribution has been given to all outside sources. I understand that I am solely responsible for obtaining any needed copyright permissions. I have obtained needed written permission statement(s) from the owner(s) of each third-party copyrighted matter to be included in my work, allowing electronic distribution (if such use is not permitted by the fair use doctrine) which will be submitted to UKnowledge as Additional File.

I hereby grant to The University of Kentucky and its agents the irrevocable, non-exclusive, and royalty-free license to archive and make accessible my work in whole or in part in all forms of media, now or hereafter known. I agree that the document mentioned above may be made available immediately for worldwide access unless an embargo applies.

I retain all other ownership rights to the copyright of my work. I also retain the right to use in future works (such as articles or books) all or part of my work. I understand that I am free to register the copyright to my work.

REVIEW, APPROVAL AND ACCEPTANCE

The document mentioned above has been reviewed and accepted by the student's advisor, on behalf of the advisory committee, and by the Director of Graduate Studies (DGS), on behalf of the program; we verify that this is the final, approved version of the student's thesis including all changes required by the advisory committee. The undersigned agree to abide by the statements above.

Rachel Kaplan, Student

Dr. Isabel C. Escobar, Major Professor

Dr. Zach J. Hilt, Director of Graduate Studies

# EXPLORING THE EFFECT OF CASTING SOLUTION COMPOSITION, ADDITIVES, AND CASTING CONDITIONS ON THE MORPHOLOGY AND SEPARATION PERFORMANCE OF PVDF MEMBRANES

---

THESIS

---

A thesis submitted in partial fulfillment of the
requirements for the degree of Master of Science in the
College of Engineering

at the University of Kentucky

By

Rachel Kaplan

Lexington, Kentucky

Director: Dr. Isabel C. Escobar, Professor of Chemical Engineering

Lexington, Kentucky

2024



https://orcid.org/0009-0007-4959-163X

ABSTRACT OF THESIS

# EXPLORING THE EFFECT OF CASTING SOLUTION COMPOSITION, ADDITIVES, AND CASTING CONDITIONS ON THE MORPHOLOGY AND SEPARATION PERFORMANCE OF PVDF MEMBRANES

Global water scarcity and quality concerns in the past decade have led to a looming global water crisis. Polymeric membranes have emerged as a potential solution due to their modularity, operational reliability, and wide range of contaminant removal. Polyvinylidene fluoride (PVDF) is often selected as a membrane material for its enhanced chemical resistance, thermal stability, and mechanical strength. However, these membranes often require more complex fabrication methods or support materials to achieve optimum performance. Flat-sheet unsupported PVDF membranes were fabricated via nonsolvent induced phase separation. The influence of solvent, polymer composition, pore forming additives, and casting conditions were explored with respect to membrane properties and performance. The efficacy of environmentally friendly solvents was explored using Rhodisaolv® PolarClean and gammavalerolactone (GVL), which are either bioderived or ecofriendly and reduced/no toxicity compared to traditional petroleum derived solvents, such as N-methyl-2-pyrrolidone (NMP). GVL was unable to dissolve PVDF as a lone solvent, but when mixed into a cosolvent with PolarClean dissolution was observed. Solutions using green solvents were more viscous than those prepared with NMP, which impacted morphology, porosity, and separation performance. The addition of polyvinylpyrrolidone (PVP) as a pore forming additive increased membrane permeability and porosity at higher concentrations; however, a decrease in selectivity was observed. Casting speed was found to have a significant effect on mechanical strength and hydrophobicity. A critical shear rate was identified where permeability and selectivity performance is optimal.

KEYWORDS: Membrane filtration, flat-sheet PVDF membranes, green solvents, polyvinylpyrrolidone, critical shear rate

Rachel Kaplan
*(Name of Student)*

06/28/2024
Date

# EXPLORING THE EFFECT OF CASTING SOLUTION COMPOSITION, ADDITIVES, AND CASTING CONDITIONS ON THE MORPHOLOGY AND SEPARATION PERFORMANCE OF PVDF MEMBRANES

By
Rachel Kaplan

Isabel C. Escobar
Director of Thesis

Zach J. Hilt
Director of Graduate Studies

06/28/2024
Date

ACKNOWLEDGMENTS

The following thesis, while an individual work, benefited from the insights and direction of several people. First, my Thesis Chair, Isabel Escobar, exemplifies the high quality scholarship to which I aspire. Next, I wish to thank the complete Thesis Committee, Zach Hilt and Eduardo Santillan-Jimenez. Each individual provided insights that guided and challenged my thinking, substantially improving the finished product. I'd also like to acknowledge my lab group for their support both inside and out of the lab.

In addition to the technical and instrumental assistance above, I received equally important assistance from family and friends. My fiancé, Ryon Bean, provided continual support throughout my entire graduate school experience. My friends, family, dog, and cats have been indispensable throughout the thesis process. I can't thank you all enough, we did it!

# TABLE OF CONTENTS

# LIST OF TABLES

# LIST OF FIGURES

# CHAPTER 1. INTRODUCTION

## 1.1 Global Water Crisis

Access to clean water is an escalating global challenge, with two-thirds (4 billion people) of the population living under conditions of severe water scarcity for at least one month of the year[1]. Current trends of human activities on the planet are set to exacerbate these already present issues. Rapid population growth is set to continue, with the largest growth occurring in areas which already experience the greatest degree of water shortage. Furthermore, industrial expansion is not only dependent on groundwater sources which are already exhausted or contaminated, but also diverts water from food production to more lucrative activities. Lastly, climate change has ensured there are no large groundwater deposits in readily accessible locations, making any new resources expensive to develop[2]. Therefore, access to clean water and sanitation is such a prevalent issue that the United Nations included it in the Sustainable Development Goals for civilization to achieve by 2050, as shown below in Figure 1.1.


Figure 1.1 United Nations Sustainable Development Goal[3].

While clean water is shown explicitly in Goal 6, many other goals shown in Figure 1.1 rely on clean water to be realized. Goals such as zero hunger, good health, life below water, and life on land are directly reliant on access to clean water. As of 2023, global rates of progress still need to increase significantly to achieve universal coverage, with a sixfold increase for drinking water, fivefold for sanitation, and threefold for hygiene. Key strategies to achieve these include investment and capacity building as well as promoting innovation and evidence-based action[3]. The need for innovative and efficient water purification technologies becomes paramount as traditional water sources become increasingly unreliable.

## 1.2 Methods for water treatment and remediation

Various physical and chemical treatments have been developed and are widely used for contaminant removal from water. Some common methods are coagulation and flocculation, distillation, ion exchange, filtration, adsorption, and disinfection.[4]. Coagulation involves adding chemical coagulants, such as alum, to water which destabilize suspended particles. These particles these aggregate into larger particles, or flocs, that are easily removed. Flocculation is a gentle mixing process that results in larger flocs to form. This is a simple process that effectively removes a wide range of contaminants; however, it requires a large and continuous supply of chemicals and produces a sludge that requires proper disposal[5].

Distillation is one of the most common separation methods, especially for desalination, and is based on differences in boiling point of the individual components. Water is boiled and differences in volatility of the contaminants in the mixture allows distillation to occur[4]. While a continuous process that removes a wide range of contaminants, distillation is also a slow process that is extremely energy intensive and requires sophisticated equipment and maintenance.

Ion exchange resins are functionalized for selective separations of ions from water and are an effective method. While the cost of running the treatment itself is low, the resins require regeneration or replacement that can become expensive. The treatment is also ineffective against non-ionic contaminants[4].

Filtration involves passing water through porous materials to remove suspended particles and microorganisms. Sand filters can be used as a porous material to remove large particles and reduce turbidity. Another porous material option is a membrane, which can separate a wide range of particle sizes.

Adsorption is usually achieved using activated carbon, which adsorbs pollutants from water. One advantage of using activated carbon for adsorption is that is can be derived from renewable feedstocks such as biomass. However, activated carbon has a limited lifespan, requiring regular replacement, and can become saturated quickly, reducing effectiveness[6].

Disinfection aims to inactivate pathogens in water using chemical agents, like chlorine or chloramines, or physical methods, such as ultraviolet radiation or ozonation. A disinfection step is required for water treatment in the United States. These are relatively simple and effective methods; however, chlorine can produce harmful disinfection by-products, UV radiation does not provide residual disinfection, and ozone treatment is costly and complex to manage[7].

## 1.3 Membranes for water separations

Membrane technology has emerged as an innovative and effective method for removing contaminants from water. Membranes offer several advantages over

conventional water purification methods. They provide high-quality water output, require lower energy consumption, and can be tailored to remove a wide range of contaminants, including microorganisms, dissolved salts, and organic compounds[8]. Membrane filtration has become the industry standard for potable reuse applications due to these reasons as well as modularity and operational reliability[9]. RO membranes have also been shown to be the most effective method of removing per- and poly- fluoroalkyl substances (PFAS), especially shorter chain PFASs such as perfluoro butanoic acid[10].

A membrane is a selective barrier that allows certain substances to pass through while retaining others, based on size, charge, or chemical affinity. Membranes used in water filtration are typically thin films composed of polymers, ceramics, or other materials[11]. The effectiveness of a membrane depends on its properties, including permeability, selectivity, and mechanical strength, which are influenced by its composition and fabrication conditions. Membranes are typically categorized by pore size, as shown below in Figure 1.2[12], which is correlated with the size of particle the membrane can reject.

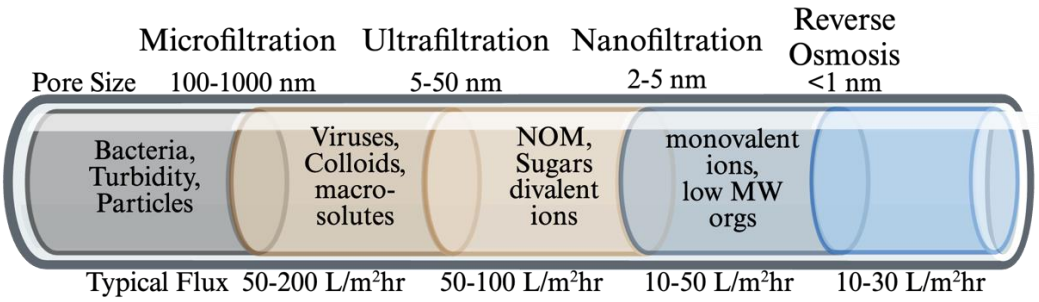


Figure 1.2 Membrane filtration regimes including pore size, typical contaminants rejected, and typical flux for water treatment applications.

Microfiltration (MF) membranes have the largest nominal pore size, between 0.1-1.0 $\mu$m, and typically reject larger particles and microorganisms[13]. Ultrafiltration membranes (UF) can reject bacteria and soluble macromolecules, such as proteins, as well as large molecules and microorganisms. Nanofiltration (NF) and Reverse Osmosis (RO) membrane processes are similarly designed such that they both remove dissolved chemical contaminants. NF membranes remove many of the same solutes as RO membranes, but to a lesser degree. RO membranes are effectively non-porous and exclude even low molecular weight species, such as ions[14]. As pore size decreases, fluid flux through the membrane also decreases and requires higher pressure during filtration. MF and UF processes are considered low pressure and mainly separate through sieving, or size exclusion, where the particles are larger than the pore diameter. NF and RO processes both require high operating pressures and separate through more complex mechanisms. In membranes processes, solutes are rejected through both exclusion and transport mechanisms. Steric, dielectric, and Donnan exclusion take place, as well as adsorption to the membrane surface in some cases. Rejection is also a function of the relative transport resistances of solutes and water, like convection and diffusion[9].

One of the main drawbacks of using membranes for water treatment is fouling. Fouling is the accumulation of contaminants on or within the membrane structure and reduces overall efficiency. As foulants accumulate on the membrane surface, membrane permeability declines and its ability to retain solutes is altered. This deteriorates membrane performance, increases operating costs, and shortens membrane life[12]. Fouling can be prevented through regular backwashing or mitigated through chemical cleaning[9]. The type of chemical used for cleaning depends on the membrane material chemical tolerance.

### 1.3.1 Membrane Materials

Membranes can be fabricated from organic materials, like polymers, and inorganic materials, like metals and ceramics. Polymeric membranes have become a popular choice for water treatment due to their unique properties and numerous other advantages over their inorganic counterparts. One advantage of polymeric membranes is cost effectiveness. Material costs of polymers versus ceramics or metals is generally lower, making it more cost effective for large scale applications[15]. The manufacturing processes for polymeric membranes are relatively less complex and costly compared to those for ceramic membranes, leading to more affordable manufacturing. This relative ease of fabrication enables the production processes of polymeric membranes to be highly scalable for the manufacture of large quantities to meet demand. Polymer based membranes can be fabricated into various forms and configurations, such as flat sheets, hollow fibers, and tubular structures, providing flexibility in designing membrane modules and systems[16]. Polymeric membranes also have a wide range of versatility and can be tailored for various water treatment processes from MF to RO. The membrane chemical composition can be further adjusted to optimize for permeability, selectivity, and mechanical strength. The innate chemical and physical properties of polymers, such as chemical resistance and hydrophobicity, can be leveraged or modified for the desired membrane application. In addition to cost efficiency, polymeric membranes also have increased energy efficiency. Compared to ceramic membranes, polymeric membranes typically operate at lower pressures, reducing energy consumption and operational costs[17]. The lower energy requirements for the operation of polymeric membrane modules contribute to a smaller environmental footprint compared to more energy-intensive alternatives. In terms of environmental impact, while some polymeric materials are recyclable, advancements in polymer technology are focusing on developing biodegradable membranes. Another avenue to reduce the environmental impact of membrane fabrication is the choice of solvent used when dissolving polymers. Developing membranes from sustainable solvents is a key research thrust for advancements in membrane fabrication.

Some conventional polymers used in membrane fabrication include cellulose acetate (CA), polysulfone (PSf), polyethersulfone (PES), polyamide (PA), and polyvinylidene fluoride (PVDF). Polysulfone is one of the most selected polymers due to

its commercial availability and ease of processing[18]. Cellulosics usually include cellulose esters, including the most common, cellulose acetate. Cellulose acetate has low chemical, mechanical, and thermal resistance and is often blended with other polymers or additives[18]. PVDF exhibits high chemical resistance, thermal resistance, and mechanical strength. PVDF is notably hydrophobic and often requires surface modification for membrane applications[19].

## 1.4 Membrane fabrication via Nonsolvent Induced Phase Separation (NIPS)

Polymeric membranes are generally fabricated through a phase inversion process, where a polymer solution is transformed from a liquid to a solid state. Prior to solidification, a liquid-liquid demixing occurs where the thermodynamically stable polymer solution demixes into a polymer-rich and a polymer-poor phase. The phase with the highest polymer content then precipitates and solidifies, through processes like gelation or crystallization, to become the solid membrane matrix[20]. The polymer-poor phase leads to pores within the solid membrane matrix. This demixing and resulting polymer precipitation can be induced through various methods.

Polymer precipitation can occur through evaporation, thermal precipitation, precipitation from the vapor phase, and immersion precipitation[20]. The evaporation method, evaporation induced phase separation (EIPS), involves the controlled evaporation of a volatile solvent from the polymer solution. Thermally induced phase separation (TIPS) involves the cooling of a homogenous polymer solution to induce phase separation. As the temperature decreases, the polymer becomes less soluble, leading to the formation of a solid membrane[20]. Vapor induced phase separation (VIPS) involves exposing a cast polymer solution to a vapor phase, usually a nonsolvent vapor, which diffuses into the polymer solution. Immersion precipitation, or nonsolvent induced phase separation (NIPS), involves immersing the polymer solution in a nonsolvent bath.

Among these methods, NIPS is the most often used technique and the focus of this work. The only requirement for the process is that the polymer be soluble in a solvent or solvent mixture, allowing a wide variety of polymers to be used in membrane fabrication[20]. EIPS requires a highly volatile solvent be used in the polymer solution and an extremely climate-controlled casting area for controlled evaporation. TIPS requires a temperature sensitive solvent and adds a temperature element to already complicated thermodynamic and kinetic systems. VIPS requires the controlled production of a nonsolvent vapor, as well as climate control during casting.

A schematic of the NIPS process for flat sheet membranes at the bench scale is shown below in Figure 1.3. The dope solution is prepared by combining the desired weight percentage of polymer in a suitable solvent and stirring for a set amount of time. Often heat is applied to aid in the dissolution. The homogenous polymer solution is then be poured on a substrate, typically a glass plate or a polymeric support, and a doctor

blade with a specific coating gap is passed over the solution. This creates a thin polymer film which is then immersed into a nonsolvent bath, usually water, where the phase inversion process takes place. The nonsolvent diffuses into the polymer film while the solvent diffuses out, leading to precipitation. Polymer choice is often based on desired physical and chemical properties for the resultant membrane application. After polymer selection, a suitable solvent-nonsolvent system for the polymer must be identified. There are many thermodynamic and kinetic aspects to consider within the NIPS process such as solution thermodynamics and diffusion kinetics.

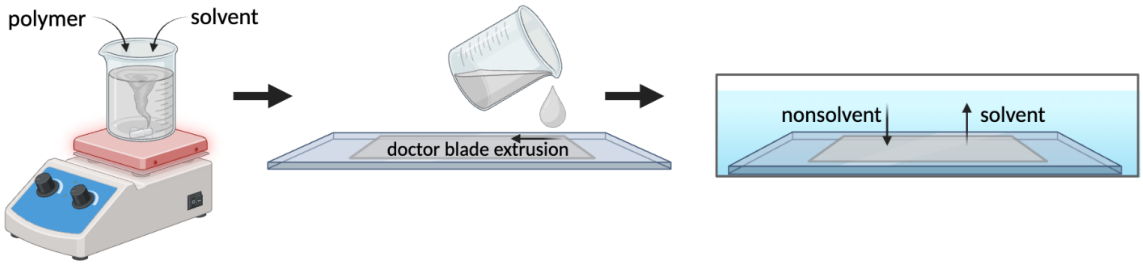


Figure 1.3 Schematic of nonsolvent induced phase separation including formation of dope solution, casting, and coagulation bath for flat sheet membranes.

### 1.4.1 Thermodynamic considerations

Strathmann proposed that a ternary phase diagram could be used as a tool to analyze the thermodynamics of the membrane precipitation process[21]. The system is composed of polymer/solvent/nonsolvent and is pictured below in Figure 1.4.

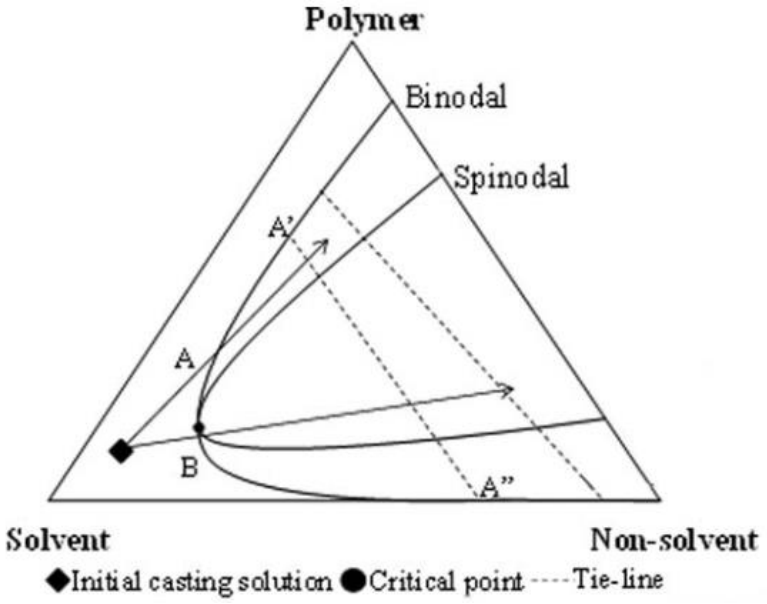


Figure 1.4 Idealized ternary phase diagram: schematic representation of phase separation mechanisms during membrane formation. Copyright liscense granted by John Wiley and Sons[21].

The ternary phase diagram consists of a single-phase region, where all components are miscible, and a two-phase region, where the system separates in polymer-poor and polymer-rich phases. The binodal curve is the liquid-liquid phase boundary and separates the two regions[18]. The initial casting solution is in a stable monophasic region of the diagram. Contact with the nonsolvent bath causes the composition of the polymer solution to move towards the polymer/nonsolvent axis, along pathways A and B, which represent binodal demixing and spinodal decomposition. The spinodal represents the boundary between metastable and unstable phases within the two-phase region. Separation by binodal demixing (pathway A) leads the polymer solution to end up in a metastable region, between the binodal and spinodal. Here demixing occurs, leading to phase separation and precipitation according to the nucleation and growth mechanism. The polymer-lean phase composition is shown as point A" and the polymer-rich phase is shown as point A'. These points are connected by a tie-line, which joins phases at equilibrium with each other. Separation by spinodal decomposition (pathway B) occurs when the composition crosses the region between the bi- and spinodal without leaving enough time to start demixing. This causes the polymer solution to end up in the unstable region inside the spinodal, either directly or via the metastable region. This causes two co-continuous phases to develop initially, which might finally transform into nuclei as with binodal demixing[22]. These two different separation pathways also result in different membrane morphologies[23].

Strathmann also observed these two distinct morphologies as a function of precipitation rate, which is the time it takes for the cast film to become opaque or separate from the substrate[24]. A slower precipitation rate, or delayed demixing, results in a "sponge-like" morphology. The cross section of these membranes shows a high presence of micro voids with little to no macro voids and a relatively dense top layer. A faster precipitation rate, or instantaneous demixing, results in large "finger-like" macro voids in the substructure[21]. Sponge-like morphology membranes tend to have lower fluxes but higher rejections for smaller sized solutes, like salt. Membranes with finger-like voids tend to perform the opposite, with higher water flux and lower solute rejection.

The most simple and direct approach to determine the thermodynamics of a system experimentally is to determine the cloud point, or precipitation, curve[25]. The cloud point curve is the border between stable and meta- or unstable regions. Systems using a monodisperse polymer can be considered truly ternary, in which the cloud point curve coincides with the binodal. Polydisperse polymers become fractionated between two phases at equilibrium, causing the polymer-rich and polymer-poor phases to not lie exactly on the binodal. Despite this, the cloud point curve still gives the best estimation of the thermodynamics of a system[20]. Cloud points are determined experimentally by visual observation of the turbidity change of polymer solutions while titrating with nonsolvent.

### 1.4.2 Kinetic considerations

The main kinetic aspect of NIPS is the diffusion rate of solvent out and nonsolvent into the cast polymer film. Faster diffusion leads to instantaneous demixing, while slower diffusion results in delayed demixing and the resultant morphologies. Ternary diffusion equations are a function of chemical potential gradient in the polymer film and frictional coefficients between the components[23]. Cohen et al. developed a model such that the flow of solvent and nonsolvent in the film can be treated as a one-dimensional diffusion process, as shown below in Figure 1.5. Here it is assumed a three-dimensional structure consisting of two interspersed phases in equilibrium will form during phase separation[26]. This allows for a polymer fixed frame of reference, described by position coordinate $m$.

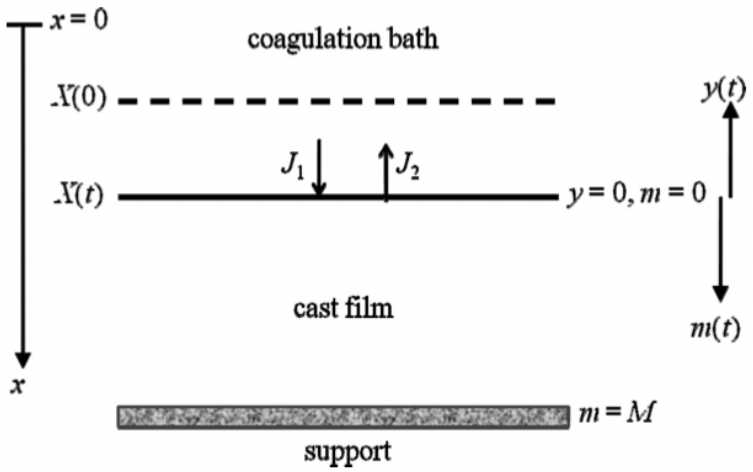


Figure 1.5 Flow of Solvent and nonsolvent treated as a one-dimensional diffusion process. Copyright liscense granted by John Wiley and Sons[26].

Radavanovic et al. then used this ideology to develop models to describe diffusion in the film and the coagulation bath with the coordinate systems defined in Figure 1.5. Describing diffusion in the film before the demixing process begins with the continuity equation, as shown below.

$$\frac{\partial\left(\frac{\phi_i}{\phi_3}\right)}{\partial t} = \frac{\partial J_i^p}{\partial m}, i = 1,2 \tag{1}$$

$$m(z,t) = \int_0^z \phi_3(x,t)\,dx \tag{2}$$

Here $J_i^p$ is the volume flux of component $i$, $\phi_i$ is the volume fraction of component $i$, $t$ is time, and $i = 1, 2, 3$ represents the nonsolvent, solvent, and polymer respectively. Fluxes are calculated using component velocities and chemical potentials. To model diffusion of each component in the film, thermodynamic and frictional contributions must be defined

between nonsolvent, solvent, and polymer. Diffusion in the coagulation bath is described by:

$$\frac{\partial v_i}{\partial t} = \frac{\partial}{\partial y}\left(D\frac{\partial v_i}{\partial y}\right) - \frac{\partial v_i}{\partial y}\frac{dX}{dt} \tag{3}$$

$$\frac{dX}{dt} = -J_1^p(0,t) - J_2^p(0,t) \tag{4}$$

where $v_i$ is the volume fraction of component $i$, $D$ is the mutual diffusion coefficient, and $X$ is the position of the interface between the film and the coagulation bath[27]. Equations 1 and 3 must be solved simultaneously to calculate the critical initial compositions at which demixing changes from instantaneous to delayed. The task of modeling diffusion in the film and coagulation bath are outside the scope of this work due to the wide range of systems studied. However, a fundamental understanding of the kinetic forces at play is key for understanding the interactions during phase inversion and the resulting membrane morphology and performance.

Several variables influence the thermodynamic and kinetic behaviors of the system during phase inversion. Viscosity of the dope solution influences the diffusion of solvent and nonsolvent in the film and therefore the rate of precipitation. Polymer concentration and solvent choice influences dope solution viscosity. The relative miscibility between solvent and nonsolvent also has an influence on the demixing behavior. These and other factors that influence the liquid-liquid demixing and polymer precipitation ultimately determine the morphology and separation performance of membranes made by nonsolvent induced phase separation.

## 1.5 Parameters influencing morphology and performance

Understanding and controlling the parameters that influence the demixing behaviors during phase inversion is essential for optimizing membrane properties for specific water treatment applications. The choice of solvent-nonsolvent systems has a significant influence on membrane morphology, mechanical properties, separation performance, and interfacial characteristics. The composition of the polymer solution including polymer choice, concentration, and additives also heavily influences the resulting membrane properties. The casting conditions including coating gap, casting speed, and evaporation time will also be discussed.

### 1.5.1 Choice of solvent-nonsolvent system

The polymer must be soluble in the chosen solvent, and the solvent and nonsolvent must be miscible. Several approaches to determine polymer-solvent solubility have been developed and extensively studied to aid in the choice of an appropriate system. Thermodynamics states that the Gibbs free energy of mixing, $\Delta G_m$, for the solution process must be negative for solution to occur, as shown in Equation 5[28],

$$\Delta G_m = \Delta H_m - T\Delta S_m \tag{5}$$

where $\Delta H_m$ is the enthalpy of mixing, T is absolute temperature, and $\Delta S_m$ is the entropy of mixing. Flory and Huggins developed a theory that uses a statistical approach within a lattice model to calculate the Gibbs free energy change of mixing a polymer with a solvent, and is calculated as follows:

$$\Delta G_m = kT(n_1 ln\phi_1 + n_2 ln\phi_2 + \chi_{12} n_1 \phi_2) \tag{6}$$

where $k$ is Boltzmann's constant, $T$ is absolute temperature, $n_1$ and $n_2$ are the number of solvent and polymer molecules respectively, $\phi$ is the volume fraction and $\chi_{12}$ is the Flory interaction parameter[18]. The Flory interaction parameter is a dimensionless characterization of polymer-solvent interaction energy and must be determined experimentally. Solubility parameters of solvents, δ, can be used to estimate $\chi_{12}$ and are calculated as follows:

$$\delta = \sqrt{\frac{\Delta E^v}{V}} \tag{7}$$

where $\Delta E^v$ is the molar energy of vaporization, and $V$ is molar volume. Hansen posed that $\Delta E^v$ includes the energies arising from all modes of interaction holding the liquid together. The three major modes of interaction contributing to the cohesive energy density include dispersion, polar, and hydrogen bonding forces. Therefore, it can be assumed the molar energy of vaporization and resulting solubility parameter are a sum of the dispersion (d), polar (p), and hydrogen bonding (h) contributions, as shown in Equations 8 and 9[29].

$$\Delta E^v = \Delta E^d + \Delta E^p + \Delta E^h \tag{8}$$

$$\delta = \sqrt{\delta_d^2 + \delta_p^2 + \delta_h^2} \tag{9}$$

Hansen then posed that a solvent's solubility parameter could be considered as a vector with components $\delta_d$, $\delta_p$, and $\delta_h$. This means each solvent can be plotted in a three-dimensional system with dispersion, polar, and hydrogen bonding axes. This is shown below in Figure 1.6.

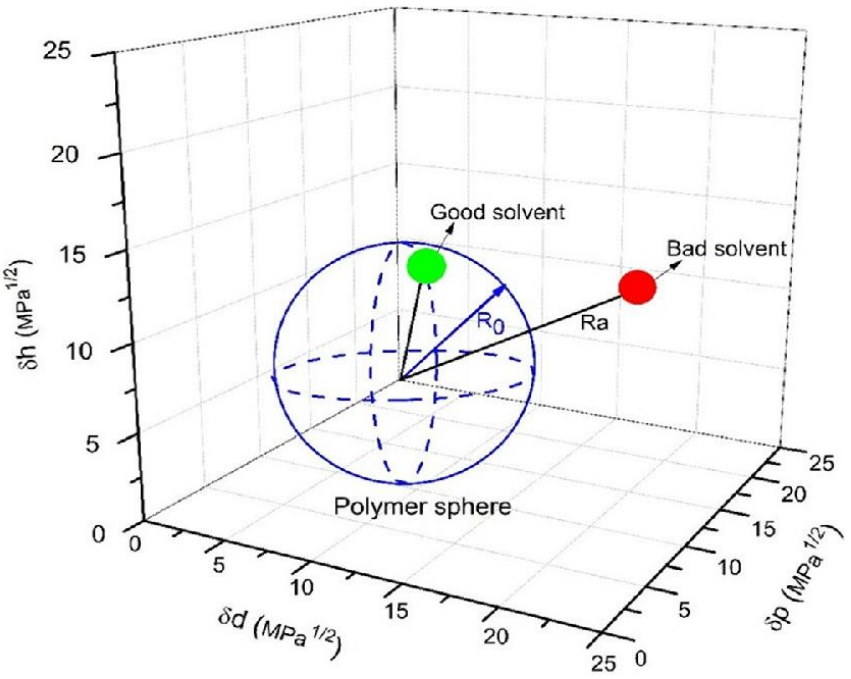


Figure 1.6 Interaction radius of the Hansen solubility sphere for the radius determination for good and bad solvents. Open access article[31].

Using this coordinate system, the relative affinity ($R_a$) between a polymer and solvent can be measured by the distance between points based on each individual Hansen solubility parameter. The radius of interaction of the Hansen solubility parameter sphere ($R_o$) quantifies the maximum distance between and solvent and polymer that will lead to solution to form. The ratio between the relative affinity and the interaction radius of the polymer determines the relative energy difference (RED). The RED should be less than 1 to maintain solubility, which increases as the RED approaches 0. This method has become widely used as a screening for potential solvents; however, solvents with an RED between 0 and 1 are only considered to be potentially compatible. Additional outside forces may be needed for complete dissolution, such as heat.

Other solvent considerations outside of solubility are volatility, miscibility with the nonsolvent, and now toxicity. Highly volatile solvents can rapidly evaporate during casting and lead to dense membrane structures in some cases. Common solvents used for membrane fabrication via NIPS up to now are n-methyl-2-pyrollidone, dimethyl sulfoxide (DMSO), dimethyl formamide (DMF), and tetrahydrofuran (THF). These are derived from petroleum processes and can be an irritant, highly flammable, and even reprotoxic[19]. Solvents are handled not only when dissolving polymers, but also during casting and after within the coagulation bath. The use of these solvents has become extremely limited in the EU, with the intention to effectively eliminate the use of NMP in consumer applications[30]. With adverse effects for both the environment and human health, efforts have turned to finding sustainable alternatives.

The nonsolvent must be miscible with the solvent but not the polymer. This miscibility impacts the rate at which the nonsolvent exchange occurs and therefore the

polymer precipitation rate. The morphology resulting from this can affect the mechanical strength of the membrane. Proper nonsolvent selection ensures a balance between mechanical strength and functional performance, making membranes suitable for high pressure applications[31]. Water is an ideal nonsolvent in many cases due to its non-toxicity and low cost.

The composition of the nonsolvent is yet another parameter that can be used to influence membrane structure and performance. Addition of solvent into the nonsolvent bath shifts the composition and pathway of the system, delaying demixing and preventing instantaneous demixing, by lowering the polymer concentration at the interface[18]. The opposite is theoretically true as well, where adding nonsolvent into the polymer solution demixing could be sped up.

### 1.5.2 Composition of polymer solution

For porous membranes, the choice of polymer affects solute adsorption, membrane hydrophilicity, and the thermal and chemical stability of the membrane. The hydrophilicity of the membrane surface affects water permeability and fouling characteristics. The choice of polymer is also important in NIPS because it limits the solvents and nonsolvents that can be used. As previously discussed in section 1.3.1, many different polymers can be used in the synthesis of membranes of various pore sizes. Polysulfone (PSf) is often the polymer of choice not only for its commercial availability and ease of processing but also its favorable selectivity-permeability characteristics and glass transition temperature ($T_g$) value of 190 ºC[18]. Polyethersulfone (PES), with $T_g = 230$ ºC, also has good chemical and thermal stability[18]. Polyacrylonitrile (PAN) is a popular commercialized membrane material for its resinous, fibrous, or rubbery morphologies and sufficient chemical stability. Its hydrophilicity is generally an advantage over other common membrane materials, like PSf and PES. However, PAN has poor solubility except in polar solvents like NMP and DMF[18].

Polytetrafluoroethylene (PTFE) and polyvinylidene fluoride (PVDF) are fluoropolymers frequently chosen for membrane fabrication. Both are hydrophobic and exhibit high chemical and thermal stability due to their crystallinity. While PVDF shows slightly lower chemical and thermal resistance, it is soluble in aprotic solvents such as NMP and DMF[18]. This high chemical resistance yet solubility with traditional solvents makes PVDF an advantageous choice for water treatment applications. It allows the ease of processibility by synthesis through NIPS and resistance to solvents used in membrane regeneration after fouling.

Despite high chemical, thermal, and mechanical stability, PVDF membranes have several notable disadvantages that can limit their applicability and performance. One of the primary challenges is their inherent hydrophobicity, which makes them prone to fouling, especially when treating aqueous solutions such as proteins and humic substances[12]. Additionally, the fabrication of PVDF membranes typically involves the

use of toxic solvents like NMP and DMF, which pose environmental and health risks[32]. Moreover, while PVDF exhibit excellent chemical resistance, their mechanical properties can be compromised under extreme pH conditions or prolonged exposure to harsh chemicals, potentially leading to membrane degradation and reduced lifespan[33]. Another significant concern is the potential leaching of per- and polyfluoroalkyl substances (PFAS) from PVDF membranes. PFAS are a group of highly persistence chemicals that can pose severe environmental and health risks due to their toxicity and bioaccumulative nature[34]. Studies have shown that PFAS can leach from PVDF membranes, contaminating the treated water and potentially impacting the benefits of using these membranes in water purification processes[35]. Despite this potential, according to a recent United States Department of Energy publication, PVDF is referred to as a polymer of low concern for its production leading to PFAS contamination[36]. Therefore, ongoing research and development efforts are focused on mitigating these disadvantages through innovative fabrication techniques, surface modifications, and the use of green solvents.

Concentration of the polymer solution is a key factor in determining the resulting membrane morphology. Typical polymer concentration ranges from 15 to 25 wt %. A higher polymer concentration in the casting implies that there is a higher volume fraction of polymer after phase separation and consequently a lower porosity[18]. Higher concentrations also result in more viscous solutions, limiting diffusion and leading to more dense membranes with smaller pores. This results in higher selectivities and lower permeabilities. The polymer concentration also influences the resultant membrane thickness which affects separation performance[37]

### 1.5.3 Additives

The addition of organic or inorganic components has become one of the most important techniques in membrane construction. Most casting solutions contain additives for improving the morphology and function, making the analysis of the system more complex. These additives can enhance pore formation, improve pore interconnectivity, and increase hydrophilicity[18]. Frequently used polymeric additives include polyvinylpyrrolidone (PVP) and polyethylene glycol (PEG). A more novel inorganic additive material is silver nanoparticles (AgNPs). PVP is a common pore-forming agent used in the NIPS process to increase the membrane's porosity and hydrophilicity. During phase inversion, PVP creates a network of pores by leaching out into the non-solvent bath, leaving behind a porous structure[38]. PEG is another widely used additive in membrane fabrication. PEG acts as a pore-forming agent like PVP but with different molecular weights, which can be tuned to control the pore size and distribution in the membrane. By adjusting the molecular weight of PEG, the pore size distribution can be finely tuned to achieve specific separation requirements. The addition of PEG generally results in membranes with higher water flux and better permeability due to formation of more interconnected pores[39].

Silver nanoparticles are incorporated into membranes to provide antimicrobial properties. AgNPs are dispersed in the polymer solution, where they integrate into the membrane matrix during phase inversion. AgNPs provide strong microbial effects, preventing the growth of bacteria and biofilms on the membrane surface. The antimicrobial properties help in maintaining membrane performance over longer periods, reducing the need for frequent cleaning and replacement[40].

The addition of another polymer species often inherently increases the viscosity of the casting solution; therefore, the amount of additive is also a factor of careful consideration. Each species interacts with each system uniquely, but the general purpose is to leach out of the casting solution during phase inversion, enhancing porosity.

### 1.5.4 Casting conditions

Once the composition of the polymer solution is decided, the conditions with which it is cast must then be determined. The thickness of the film, the speed of the casting knife, and how long the cast film spends in air before immersion all can affect the morphology and performance of the membrane. The wet thickness of the film is determined by the coating gap of the casting knife. This is the distance between the edge of the knife and the substrate, usually on the scale of micrometers. The wet thickness may differ from the thickness of the final membrane due to casting speed, the rheological properties of the solution, and the surface properties of the support[41]. These parameters can cause shrinkage of the cast film after phase inversion. From a fundamentals point of view, the thickness of the film affects the diffusion of solvent and nonsolvent; therefore, the demixing rate and morphology. Some studies find that higher coating gaps and thicker wet thickness membranes show more macrovoid formation. The mechanisms are not well understood, but evidence suggests there is a critical-structure transition for systems during the phase inversion process in which the properties of the membrane within this region are significantly changed[41]. This possibly stems from the different ways polymer conformation changes in the solidifying film and the accompanying built-up forces that can impact areas of the film still undergoing solidification.

The rate at which the casting knife passes over the dope solution also affects the membrane architecture. Phase inversion typically involves casting a shear-thinning and viscoelastic solution, where the solution is subjected the shear stress before undergoing rapid coagulation. The shear-thinning behavior of the polymer solution indicates a progressive alignment of polymer molecules in the direction of flow. Consequently, this shear-induced molecular orientation has beneficial effects on the separation properties of the resulting membrane, to a certain limit[42]. Polymer molecules are in a partially oriented conformation down the castline during casting, then potentially relax to some preferred state before immediate immersion. The immediate immersion limits conformational rearrangement, especially in the newly formed skin region. This results in a well-defined skin layer with enhanced molecular orientation, directly affecting the

surface pore radius and membrane separation ability[42]. This is usually beneficial until the critical shear rate is reached, which is the maximum point in which the resultant membrane exhibited optimal performance, morphology, and provides the best structural properties. Beyond the critical shear rate, the separation performance of the membrane tends to decline[43]. The shear rate experienced during casting is calculated as follows[44]:

$$shear\ rate\ (s^{-1}) = \frac{velocity\ of\ casting\ knife\ \left(\frac{m}{s}\right)}{membrane\ thickness\ (m)} \tag{10}$$

The formation of a selective skin layer is a commonly used practice in the synthesis of asymmetric membranes. One of the simplest ways to enhance skin layer formation is the introduction of an evaporation step before immersion in the coagulation bath. During this step, the volatile solvent evaporates, starting at the polymer film-air interface, and begins to phase invert. This forms a skin layer with a locally increased polymer concentration, which acts as a barrier after immersion, during diffusion, and results in delayed demixing[20]. Parameters such as evaporation time, temperature, and the relative humidity of the air during exposure all impact the specific morphology of the selective layer.

## 1.6 PVDF membranes

As previously discussed, the properties of PVDF make it an advantageous membrane material. Due to its high chemical resistance, thermal stability, mechanical strength and hydrophobicity, PVDF has been used extensively in ultrafiltration and microfiltration membranes. PVDF is resistant to a wide range of chemicals, including acids, bases, and organic solvents, making it suitable for treating different types of wastewater in harsh environments[45]. PVDF membranes can operate at higher temperatures compared to many other polymeric membranes, which is beneficial for processes involving hot fluids or thermal sterilization. The high tensile strength and durability of PVDF membranes allow for long-term operation under various pressure conditions without significant deformation or damage. PVDF is inherently hydrophobic, which may be advantageous for certain applications but may require surface modification to enhance water permeability and fouling resistance[38]. For some applications, such as membrane distillation, high hydrophobicity is preferred. PVDF-hexafluoropropylene (HFP) is a common block co-polymer used in these applications. PVDF-HFP is more soluble, less crystalline, and has a lower glass transition temperature due to the inclusion of the amorphous HFP blocks. The increased fluorine content also enhances its hydrophobicity[46]. The incorporation of HFP groups forms highly polarized C-F bonds, which leads to increased chemical stability and mechanical strength compared to PVDF alone[47]. This can be leveraged in membrane fabrication for a more stable membrane matrix.

PVDF is a semicrystalline polymer with a degree of crystallinity ranging between 35-70%. Polymer crystallinity and the resultant membrane morphology are important factors in determining the mechanical strength properties. PVDF chains can crystallize into at least 4 distinct phases, or forms: $\alpha$ (form II), $\beta$ (form I), $\gamma$ (form III), $\delta$ (form IV)[38]. The most common and kinetically stable polymorph is $\alpha$-phase (form II), while the $\beta$ form is the most thermodynamically stable[48]. These various polymorphs favor different crystal morphologies which could affect the microstructure and surface morphology of PVDF membranes. Determination of the crystalline phases present can be done using Fourier transform infrared (FTIR) spectroscopy and X-ray diffraction (XRD)[49]. Many variables influence the crystallization of PVDF such as molecular weight, polymerization method, and thermal history. Lin et al. found morphology to be directly related to dope solution dissolution temperature[50]. Membranes from solutions formed at lower temperatures (50 ºC) had a globule size between 0.2-0.6 micron. The globule size reflects the nucleation density of PVDF crystals during precipitation and is an indication of degree of crystallinity. Membranes from solutions formed at higher temperatures (110 ºC) had a globule size as large as 10-50 micron, suggesting a considerable increase in degree of crystallinity[51]. The degree of crystallinity can be determined by measuring the specific volume of crystalline and amorphous phases[50].

The various polymorphs of PVDF impart different thermal, electric, and elastic properties to the material, The $\alpha$ phase is nonpolar, the $\beta$ phase is polar, and the $\gamma$ phase is polar but weaker than the $\beta$ phase due to the prescence of a gauche bond in every fourth C-C unit[48]. The $\delta$ phase is a polar variant of the $\alpha$ phase. Polarity is anticipated to affect the fouling behavior of the membranes. It is important to note that the characteristic properties of $\beta$-PVDF are challenging to maintain at high temperatures because the restricted orientation of the polymer chains can easily become disoriented. The crystals of the $\gamma$ phase exhibit high resistance to solvents and electron beams; for instance, they do not convert to an amorphous form even after 10 minutes of exposure, while the crystals of the $\alpha$ phase are preserved for only 0.5 minutes[48]. This property can be leveraged to enhance the durability of PVDF membranes, especially under harsh conditions.

Being a semicrystalline polymer, PVDF has a more complicated phase separation behavior than an amorphous polymer like polysulfone. Figure 1.7 illustrates the ternary phase diagrams of PVDF/NMP/nonsolvent systems at 25 ºC, constructed using cloud-point measurements. The gelation boundary for the PVDF/NMP/water system is closer to the polymer-solvent axis compared to other nonsolvent systems. This indicates only a small amount of water is needed to disrupt the solution system equilibrium and induce polymer precipitation. This suggests that the thermodynamic stability of the PVDF/NMP/nonsolvent system follows the sequence: water < methanol < ethanol < IPA. Therefore, water acts as a strong nonsolvent, while alcohols are considered weak nonsolvents for the PVDF/NMP system[38].

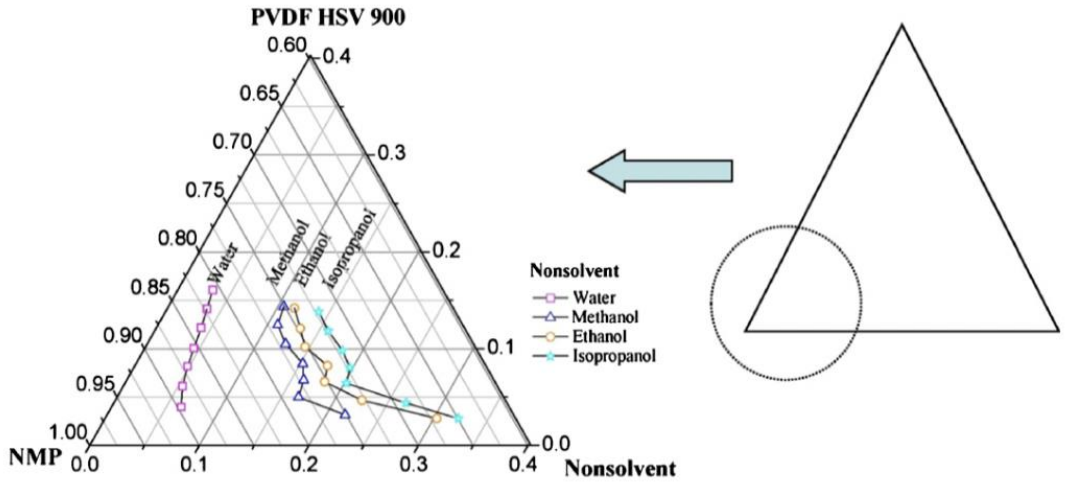


Figure 1.7 Phase diagram of ternary PVDF/NMP/nonsolvent systems at 25 ºC. Copyright liscense granted by Elsevier[40].

The inherent hydrophobicity is another consideration when choosing PVDF to fabricate membranes for water separations. The hydrophobic nature of PVDF membranes makes them prone to fouling when treating aqueous solutions containing natural organic matter, such as humic acids. Humic acids tend to readily adsorb onto the membrane surface or clog the pores, leading to reduced permeability and compromised separation performance. Fouling shortens the membrane lifespan and results in higher operation costs due to the need to frequent replacement and maintenance of the membrane modules. There are two common practices for hydrophilic modification to avoid these issues: surface and blending modifications. Surface modification is typically accomplished by coating or grafting a functional layer onto the membrane surface, with most modifications occurring on the top and/or bottom surfaces rather than inside the pores due to the limited diffusion capacity of the modifying agents. Blending modification, on the other hand, integrates the desired functional properties during membrane fabrication, allowing both preparation and modification to be completed in a single step. This method provides the opportunity to modify both the membrane surfaces and internal pores simultaneously through the synergistic interaction between PVDF and compatible solvents[38]. This will be the modification method the rest of this work focuses on.

Polyvinylpyrrolidone (PVP), polyethylene glycol (PEG), and poly (methyl methacrylate) (PMMA) are the three main hydrophilic polymer additives commonly used for blending with PVDF. In the modification and preparation of PVDF membranes via non-solvent induced phase inversion, PVP and PEG primarily act as pore-forming agents rather than hydrophilic agents, due to their water solubility and tendency to be washed out during membrane preparation and operation[52]. These additives also influence the thermodynamics and kinetics in the casting solution, controlling morphology, pore size, and pore size distribution. The influence of low molecular weight inorganic salts as pore forming additives in PVDF membranes has been studied, with lithium chloride (LiCl) being one such additive. At low concentrations (<7.5 wt.%), LiCl has been found to enhance liquid-liquid demixing due to its solubility in water[53]. At higher

concentrations, above 7 wt.%, LiCl enhanced the viscosity of the solution such that kinetic interactions dominated and prevented macrovoid formation.

On the other hand, PMMA has enhanced compatibility with the PVDF matrix and water insoluble. Nunes and Peinemann found that blending PVDF with PMMA produces membranes with varying degrees of hydrophilicity. Increasing PMMA content in the blend to 50% improved permeate quality compared to PVDF membranes without PMMA and a similar average pore sizes. This can be attributed to a more hydrophilic membrane, and confirmed by a decreased contact angle. However, when the PVDF concentration is reduced to 8.5%, the same as PMMA, macrovoids form below the selective surface, causing the membrane structure to collapse during filtration, which results in lower permeability[54].

As for the effect of solvent on PVDF systems, Bottino et al. identified eight effective organic solvents out of forty-six that were screened using the Hansen solubility parameter. Among these, N,N-dimethylacetamide (DMAc), N,N-dimethylformamide (DMF), NMP, and DMSO are commonly used as high boiling point strong solvents[33]. Yeow et al. demonstrated that the type of solvent used during the casting of PVDF flat sheet membranes significantly influences the resulting membrane structures. When using triethyl phosphate (TEP) as the solvent and water as the coagulant, a uniform sponge-like symmetric structure is formed throughout the membrane cross-section. This structure was attributed to TEP's relatively weak solvent power compared to NMP, DMAc, and DMF. This weaker solvent power allows even a small amount of non-solvent to induce phase separation, leading to early liquid-liquid phase separation. Additionally, the mutual affinity between TEP and water is relatively weak compared to other solvents examined, which favors the formation of a sponge-like membrane structure[55].

Considering the hazards of traditional solvents used in membrane fabrication, a few studies have tried to fabricate PVDF membranes from more environmentally friendly solvents, or green solvents. The term "green solvent" refers to a solvent that is either sustainably derived and/or lower in toxicity compared to traditional solvents. Two green solvents this work will be investigating are $\gamma$-valerolactone (GVL) and Rhodiasolv® PolarClean. GVL is produced from renewable lignocellulosic biomass, making it biodegradable and nontoxic[56]. PolarClean is an environmentally friendly solvent industrially produced by valorizing 2-methylglutaronitrile (MGN), a byproduct of Nylon-66 production[57]. The strong intermolecular forces in PVDF due to its semicrystalline nature can make it difficult for dissolution to occur. Despite low $R_a$ values, GVL has shown no solubility with PVDF, as experimentally observed [58]. PolarClean has been used to fabricate PVDF hollow-fiber membranes via TIPS, PVDF flat sheet membranes via a combined N-TIPS process, and PVDF-hexafluoropropylene (HFP) copolymer flat sheet membranes via a combines VIPS/NIPS technique[59-61]. Preparation of PVDF flat sheet membranes using a green solvent via only immersion precipitation has yet to be reported.

In addition to the considerations discussed above, there is a notable gap in literature for optimized PVDF flat sheet membranes using solely NIPS, without a support layer. Flat sheet PVDF membranes are often reinforced with a porous support layer, often made of materials like polypropylene or polyester[62]. This support layer provides structural integrity and enhances the overall performance of the membrane. Supported PVDF membranes have a more uniform pore structure compared to unsupported membranes, typically achieved through the support material. This structure contributes to better flux rates and mechanical robustness[62]. The support layer also enhances mechanical strength and stability, making them less prone to damage during handling and operation. In addition, the support layer helps to reduce shrinkage of the membrane structure, which influences total porosity[63]

In contrast, the inherent mechanical fragility of unsupported membranes makes them prone to physical damage, including tearing and deformation, especially under high-pressure conditions typically encounter in filtration systems. Unsupported membranes often lack sufficient tensile strength and flexibility. This can lead to difficulties during handling and installation, as well as potential failure during operation due to mechanical stress[62]. The process of fabricating unsupported PVDF membranes is more complex and delicate compared to supported membranes. Unsupported membranes must be carefully cast and dried to avoid defects such as pinholes, uneven thickness, and weak spots. This necessitates highly controlled environments and can be less forgiving of variations in the fabrication process.

## 1.7 Objectives

The overall objective of this thesis was to identify and optimize a suitable ternary system to synthesize PVDF flat sheet membranes for future applications in composite membrane configurations. Specific objectives include the following:

1. Determine the influence of polymer solution composition on membrane morphology and separation performance, with respect to polymer concentration, solvent choice, and inclusion of additives. Two different polymers were explored, PVDF and PVDF-HFP, polymer concentration was varied from 12-17 wt.% PVDF; PolarClean, GVL, and NMP were assessed as solvents; LiCl and PVP were explored as pore forming additives.
2. Investigate the influence of casting conditions on membrane morphology and separation performance, with respect to casting speed. Casting speeds explored were 300, 500, 700, and 900 cm/min.
3. Characterize membranes for pure water permeability, protein rejection, morphology, and surface chemistry. Theoretical solubility calculations were performed for solvent screening. Dope solution viscosities were characterized with respect to solvent, polymer concentration, and the inclusion of additives. Membrane structure was analyzed with Fourier transform infrared

spectroscopy (FTIR), scanning electron microscopy (SEM) images, water contact angle measurements, and porosity measurements. Membrane operation was characterized for flux and selectivity.

# CHAPTER 2. METHODOLOGY

## 2.1 Materials

PVDF Kynar® 761 (MW: 400-500 KDa; melting point: 165-172°C) and PVDF-HFP Kynar Flex® 2801-00 (MW: 400-500 KDa; melting point:140-145°C) were kindly supplied by Arkema Inc (Colombes, France). Lithium chloride (MW:42.39 KDa) and polyvinylpyrrolidone (MW:40,000 KDa) were purchased from VWR Chemicals (Solon, OH). Rhodiasolv® PolarClean was kindly provided by Solvay. $\gamma$-valerolactone (GVL, Reagent-Plus®, 99%) was purchased from Sigma-Aldrich (Fair Lawn, NJ). N-methyl-2-pyrollidone (NMP) and bovine serum albumin (BSA) were obtained from VWR Life Sciences (Radnor, PA). Deioninzed water (resistivity: 18.2 mΩ) was provided by the Chemical Engineering Undergraduate Laboratory at the University of Kentucky.

## 2.2 Thermodynamic study

### 2.2.1 Hansen solubility study

Using the Hansen solubility sphere theory, the relative affinity between a polymer and solvent, $R_a$, was calculated as follows:

$$R_a = \sqrt{4(\delta_{d2} - \delta_{d1})^2 + (\delta_{p2} - \delta_{p1})^2 + (\delta_{\mathrm{h}2} - \delta_{\mathrm{h}1})^2} \tag{11}$$

where $\delta_d$, $\delta_p$, and $\delta_{\mathrm{h}}$ represent the dispersion, polar, and hydrogen bonding parameters, respectively; 1 and 2 represent the polymer and solvent components. The relative energy difference, $RED$, between polymer and solvent is found using equation 12 below, where $R_o$ represents the interaction radius of the polymer sphere[64].

$$RED = \frac{R_a}{R_o} \tag{12}$$

In a cosolvent system, the respective contribution from each solvent towards the dispersion, polar, and hydrogen bonding force parameters can be calculated using the volume fractions, $V_i$, of the solvent mixture, as shown below in equations 13-16. Volume fractions were calculated for each species using equation 13, where $W_i$ represents weight fraction and $\rho_i$ represents density of the respective species[65].

$$V_i = \frac{\frac{W_i}{\rho_i}}{\frac{W_1}{\rho_1} + \frac{W_2}{\rho_2}} \tag{13}$$

$$\delta_d = V_1\delta_{d1} + V_2\delta_{d2} \tag{14}$$

$$\delta_p = V_1\delta_{p1} + V_2\delta_{p2} \quad (15)$$

$$\delta_h = V_1\delta_{h1} + V_2\delta_{h2} \quad (16)$$

### 2.2.2 Cloud point curve

Cloud point curve determination was conducted using the titration method[25]. Solutions of varying polymer weight percent were prepared using NMP as the solvent and allowed to stir for 24h for full polymer dissolution. PVDF solutions included 8, 10, 12, 14, and 16 wt.% in NMP and PVDF-HFP solutions included 10,12, 14, 16, and 18wt.% in NMP[61]. These solutions were then titrated with deionized water while being continuously stirred at room temperature until turbidity was observed. The solutions were then allowed to stir for an additional 24h to ensure cloud point had been reached. The known values of polymer weight, solvent volume, and microliters of water added were then converted to volume percentages. The ternary phase diagram was plotted using OriginPro.

## 2.3 Dope solution study

### 2.3.1 Preparation

Dope solutions were prepared by dissolving the desired polymer weight percentage in the desired solvent or cosolvent solution. All solutions were allowed to stir at 200 rpm for at least 24 hours before casting[66]. In total 10 solutions were prepared, tabulated as M1-M10 in Table 2.1 below. For M1-M3, polymer choice was PVDF, and concentration was kept to 15 wt.%. Solvent for each solution was varied between PolarClean, GVL, and a 3:1 cosolvent mixture of PolarClean and GVL. LiCl was included in each solution as a pore forming additive. Solutions for M1-M3 were heated to 80 ºC for the entire duration of dissolution[61]. M4-M6 dope solutions also included PVDF but varied concentration between 12, 15, and 17 wt.%. Solutions were prepared with NMP as the solvent and no pore forming additives were included. M7-M9 then kept a PVDF concentration of 17 wt.% and varied the addition of PVP between 0.5, 0.75, and 1 wt.% in NMP[53]. The influence of a PVDF copolymer was then explored with the M10 solution at a concentration of 17 wt.% PVDF-HFP and 0.5 wt.% PVP in NMP[45]. This solution was also used to explore the effect of casting conditions[67]. All solutions prepared with NMP as a solvent were dissolved at room temperature.

### 2.3.2 Dope solution characteristics

Viscosity of the dope solutions was measured using a rheometer (AG-G2, TA Instruments). Dope solutions (M4 - M10) were characterized for viscosity under a shear rate range of 0-600 $s^{-1}$. The rheological behavior of solutions made with green solvents was explored by preparing seven dope solutions of increasing PVDF concentration (8-20 wt.%). All solutions included 1 wt.% of LiCl as a pore former and were dissolved in PolarClean. Viscosity was characterized under a shear rate range of 0-10 1/s.

## 2.4 Membrane formations

Membranes were formed via doctor blade extrusion (DBE) wherein the dope solution was poured onto a glass substrate then extruded into a thin film as a doctor blade was passed over the solution, as shown in Figure 1.4[63]. The coating gap was maintained at 250 $\mu$m for all fabricated membranes[64]. The "standard" casting method described in this work includes casting the membranes into a thin film via handheld doctor blade. That is, the doctor blade was manually moved across the substrate. "Standard automatic" casting refers to the use of an automatic film coater. This device uses an automated trolley to push the doctor blade across the substrate surface at a controlled rate. The cast film and glass substrate were then immersed into a nonsolvent bath of water and allowed to phase invert. Once phase inversion was complete, the membranes were stored in a DI water bath for at least 24 hours prior to testing. Membrane compositions and casting conditions are shown below in Table 2.1.

| **Weight %** | **M1** | **M2** | **M3** | **M4** | **M5** | **M6** | **M7** | **M8** | **M9** | **M10** | **M11** | **M12** | **M13** |
|---|---|---|---|---|---|---|---|---|---|---|---|---|---|
| **Polymer** | | | | | | | | | | | | | |
| PVDF | 15 | 15 | 15 | 12 | 15 | 17 | 17 | 17 | 17 | | | | |
| PVDF-HFP | | | | | | | | | | 17 | 17 | 17 | 17 |
| **Solvent** | | | | | | | | | | | | | |
| PolarClean | 84 | | 63 | | | | | | | | | | |
| GVL | | 84 | 21 | | | | | | | | | | |
| NMP | | | | 88 | 85 | 83 | 82.5 | 82.25 | 81 | 82.5 | 82.5 | 82.5 | 82.5 |
| **Additive** | | | | | | | | | | | | | |

| | | | | | | | | | | | | | |
|---|---|---|---|---|---|---|---|---|---|---|---|---|---|
| LiCl | 1 | 1 | 1 | | | | | | | | | | |
| PVP | | | | | | | 0.5 | 0.75 | 1 | 0.5 | 0.5 | 0.5 | 0.5 |
| **Casting Conditions** | S* | S | S | S | S | S | SA* | SA | SA | SA | 700 cm/min | 500 cm/min | 300 cm/min |

TABLE 2.1 MEMBRANE COMPOSITIONS AND CASTING CONDITIONS. S* REPRESENTS STANDARD CASTING CONDITIONS VIA HANDHELD BLADE. SA* REPRESENTS STANDARD AUTOMATIC CASTING CONDITIONS VIA AUTOMATIC FILM COATER SET TO A SPEED OF 900 CM/MIN.

## 2.5 Membrane characterization

### 2.5.1 Structure

Fourier transform infrared (FTIR) spectra were obtained on a 7000e FTIR spectrometer, with attenuated total reflectance sampling technology (Varian Inc., Palo Alto, CA, USA). The scanning range was 400-4000 $cm^{-1}$ and the resolution was 8 $cm^{-1}$[68]. Membrane porosity was determined using a gas pycnometer (Accupyc 1330, Micrometrics, Norcross, GA, USA). Four coupons with a 2.54-cm radius were measured simultaneously with a helium feed pressure of 0.206 bar. Membrane volume was measured by determining change in pressure due to displacement in a constant volume[69].Total porosity was calculated by subtracting the ratio of volume measured by the pycnometer and volume based on sample geometry from 1[63]. Porosity was confirmed using the traditional gravimetric method. Membranes cut to 0.5 $in^2$ were measured for thickness and weighed before soaking in DI water for 24 hours. The total porosity was calculated using equation 17,

$$Porosity\ (\%) = \frac{W_{wet} - W_{dry}}{V_{dry} * \rho_{water}} \tag{17}$$

where $W_{wet}$ is the weight of the sample after soaking, $W_{dry}$ is the weight of the sample dry, $V_{dry}$ is the volume of the dry sample, and $\rho_{water}$ is the density of water[70]. Mechanical strength was tested on a 5K Instron with a load cell of 5 kN. Extention rate was set to 5 mm/min. Contact angle of a water droplet on the surface of the membranes was measured using a drop shape analyzer (DSA 100S, Kruss Scientific). One droplet of DI water, with a volume of 12 $\mu$L, was placed on the surface of the membrane via pipet and 10 contact angle measurements were collected over a 1 second interval. Values were then averaged and reported with standard deviation.

### 2.5.2 Morphology

Membrane morphology was determined via SEM (Quanta FEG-250) imaging of the membrane surface to determine pore size and the membrane cross section to determine

the pore morphology. Sample preparation included freeze drying and fracturing in liquid nitrogen. Samples were then mounted, and sputter coated (Leica ACE 600 sputter-coater, Leica Microsystems, Wetzlar, Germany) with platinum to a thickness of 4 nm. For samples mounted for cross-sectional imaging, the portion of sample in contact with the holder was coated with a layer of colloidal graphite (alcohol base).

### 2.5.3 Operation and performance

All filtration studies were performed in a dead-end filtration cell (Amicon Stirred Cell 50 mL, UFSC05001, Millipore Sigma) at a constant pressure of 4.137 bar (60 psi). Samples underwent 10 intervals of precompaction, where DI water was used as the feed solution. The amount of time to collect 5 mL of retentate was measured for each interval. This flowrate is used to calculate flux of water through the membrane via the following relationship:

$$flux\ [LMH] = \frac{V\ [L]}{A_{cs}[m^2] * t_V[hr]} \tag{17}$$

$V$ represents the volume of retentate, $A_{cs}$ represents the cross-sectional area of the membrane, and $t_V$ represents the time required to collect the specific volume of retentate. Flux is then normalized with respect to the pressure that is applied to drive the solution through the membrane. A bovine serum albumin (BSA) solution at a concentration of 100 ppm was filtered through the membranes for 10 intervals. The permeate from these intervals was collected then analyzed using a UV/Vis spectrophotometer (UV-6300PC, VWR International). The absorbance of the feed BSA solution and all filtration intervals was measured and used to calculate BSA rejection. Retention is calculated as follows:

$$R = 1 - \frac{c_p}{c_f} \tag{18}$$

where $c_p$ is the concentration of solute in the permeate and $c_f$ is the solute concentration in the feed. This is then reported as a percentage of solute rejected by the membrane.

# CHAPTER 3. RESULTS AND DISCUSSION

## 3.1 Theoretical Hansen solubility determination

Hansen solubility parameters for PVDF[59], PVDF-HFP[71], PolarClean, GVL[72], and NMP[73] were acquired from literature based on the Hansen solubility sphere as discussed in section 1.5.1[28]. Dispersive, polar, and hydrogen-bonding force-based solubility parameters are shown below in Table 3.1. The relative affinity was calculated using equation 11 and the RED between polymer and solvent was calculated using the relationship in equation 12.

TABLE 3.1 HANSEN SOLUBILITY PARAMETERS FOR PVDF WITH POLARCLEAN, GVL, 3:1

| Polymer | $\boldsymbol{\delta_d (MPa^{0.5})}$ | $\boldsymbol{\delta_p (MPa^{0.5})}$ | $\boldsymbol{\delta_h (MPa^{0.5})}$ | $\boldsymbol{R_o (MPa^{0.5})}$ | |
|---|---|---|---|---|---|
| a) PVDF | 17.2 | 12.1 | 10.2 | 9.6 | |
| b) PVDF-HFP | 14.6 | 11.9 | 11.4 | 8.1 | |
| Solvent | $\boldsymbol{\delta_d (MPa^{0.5})}$ | $\boldsymbol{\delta_p (MPa^{0.5})}$ | $\boldsymbol{\delta_h (MPa^{0.5})}$ | $\boldsymbol{R_a (MPa^{0.5})}$ | RED |
| PolarClean | 15.8 | 10.7 | 9.2 | a) 3.3<br>b) 3.4 | a) 0.36<br>b) 0.42 |
| GVL | 19.0 | 16.6 | 7.4 | a) 6.1<br>b) 11 | a) 0.63<br>b)1.3 |
| 3:1 PolarClean:GVL | 16.6 | 12.2 | 8.8 | a) 1.9<br>b) 4.7 | a) 0.20<br>b) 0.59 |
| NMP | 18 | 12.3 | 7.2 | a) 3.4<br>b) 8.0 | a) 0.35<br>b) 0.98 |

The relative affinity values have been calculated between PVDF, PVDF-HFP, and the neat solvents, as well as a 3:1 PolarClean to GVL cosolvent combination. GVL as a lone solvent resulted in a RED value of 0.63 of PVDF and 1.3 for PVDF-HFP, the highest values of any solvent screened. While 0.63 is below the solubility threshold of 1, GVL alone cannot dissolve PVDF, as shown in literature, likely due to the inherent crystallinity and significant differences in polar and hydrogen bonding forces. This also highlights the limitations of the Hansen solubility parameter group contribution method. This method takes many of the thermodynamic interactions into account but overlooks dissolutions kinetics. The addition of heat is often used to increase solubility; however, with PVDF being semicrystalline, the dissolution temperature will also influence the degree of crystallinity within the membrane.

PolarClean, as a neat solvent, can dissolve PVDF and PVDF-HFP with a RED value of 0.36 and 0.42. Utilizing a cosolvent combination can be advantageous to leverage the properties of two different solvents. By combining the solvent affinity of PolarClean and PVDF, the 3:1 cosolvent mixture with GVL achieves the lowest RED value among all the solvent tested, even outperforming the traditional and widely used NMP (RED = 0.35 (PVDF), 0.98 (PVDF-HFP)). This indicates the cosolvent mixture could be a promising solvent for PVDF and PVDF-HFP. This cosolvent technique, specifically with PolarClean and GVL was explored previously to dissolve PSf [64]. The inclusion of GVL in different ratios in the dope solution was found to decrease solution viscosity, and influence morphology and permeability. In this study, GVL was also unsuccessful in dissolving PSf as a lone solvent.

The limitations of the group contribution method are also highlighted by the high RED value for PVDF-HFP using NMP as a solvent. NMP has been widely used for PVDF and PVDF-HFP membrane fabrication. PVDF-HFP also generally is more soluble than PVDF due to decreased crystallinity, which is not reflected through the Hansen solubility parameters.

## 3.2 System thermodynamics

To better understand the thermodynamics, cloud point diagrams were constructed using PVDF and PVDF-HFP copolymer dissolved in NMP, titrated with water as the nonsolvent. The ternary phase diagram is shown below in Figure 3.1. The PVDF cloud point curve was conducted in triplicate and corresponded with curves found in literature[38]. The relative linearity of this curve indicates that the amount of water required to induce phase separation increases linearly with polymer concentration, as expected[74]. This is likely due to solution viscosity increasing because of increased polymer concentration, and therefore, slower diffusion rates. The cloud point curve of the co-polymer system is shifted towards the polymer/nonsolvent axis; that is, the composition path increased, indicating that a greater amount of water is required to destabilize the solution and induce demixing. This shift shows the co-polymer produces a more thermodynamically stable solution under the set conditions.

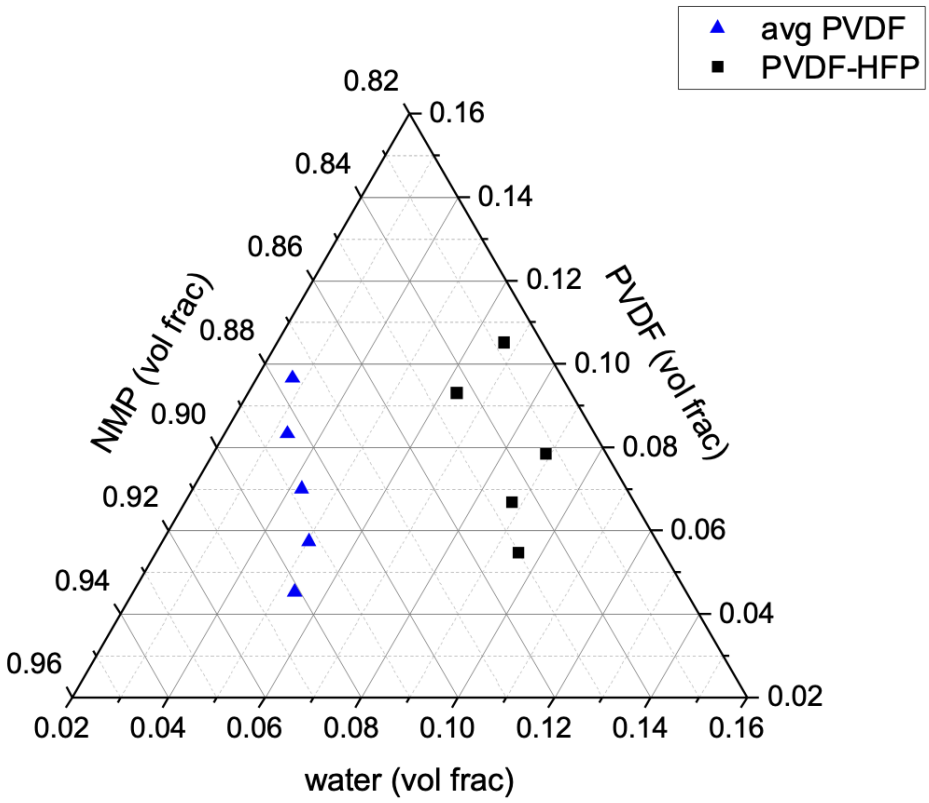


Figure 3.1 Ternary phase diagram of a PVDF/NMP/water and PVDF-HFP/NMP/water system

## 3.3 Dope solution characteristics

Viscosity as a function of shear rate for solutions of increasing PVDF concentration is shown below in Figure 3.2a. All solutions included 1 wt.% LiCl as a pore forming additive and used PolarClean as a solvent. Shear rate range was 0-10 1/s and PVDF concentrations tested were 8, 12, 14, 16, 18, and 20 wt.%. Solution viscosities at a shear rate 10 1/s are plotted in Figure 3.2b. From the trendline, and associated $R^2$ value of 0.996, viscosity increased exponentially as polymer concentration linearly increased. This corresponds with trends found in literature and is expected[75]. As polymer concentration increases, as does the degree of polymerization of the solution which inherently increases viscosity.

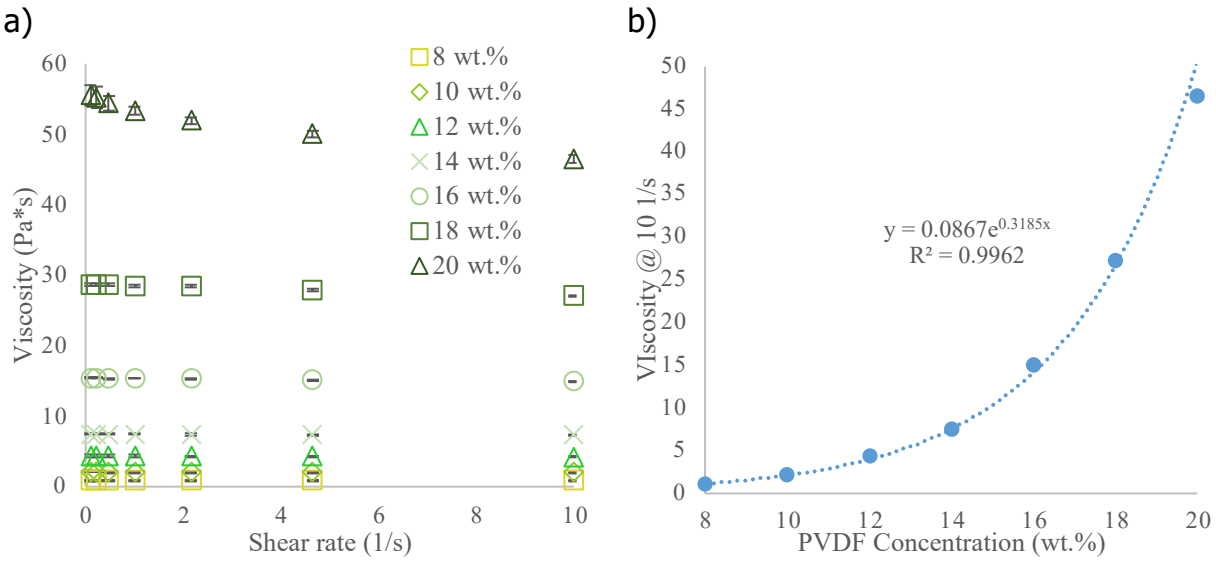


Figure 3.2 a) Dope solution viscosities as a function of shear rate from 0-10 1/s. PVDF concentration was varied from 8-20 wt.%, 1 wt.% LiCl included as pore forming additive, dissolved in PolarClean b) Viscosity at a shear rate of 10 1/s plotted as a function of PVDF concentration, including exponential trendline equation and coefficient of determination.

Attempts at dissolution of PVDF using GVL as a lone solvent were unsuccessful. Even under elevated temperature, the solution gelled and did not achieve complete dissolution and was not included in characterization. Viscosities of dope solutions used to prepare membranes M4 - M13 are plotted over a shear rate range of 6-600 1/s in Figure 3.3a. All solutions used NMP as a solvent and membranes 10-13 were cast from the same solution, referred to as M10. Viscosity at a fixed shear rate of 10 1/s are tabulated in Figure 3.3b. It is important to note the difference in scale between Figure 3.2 and 3.2. Solutions made from PolarClean had much higher viscosities in comparison to those made from NMP. The solution composed of 12 wt.% PVDF and 1 wt.% LiCl in PolarClean had a viscosity of 4.32 ± 0.145 at a shear rate of 10 1/s, which is significantly higher than the solution composed of 12 wt.% PVDF in NMP with a viscosity of 0.579 ± 0.107 at the same shear rate. PolarClean is reported to have a dynamic viscosity of 9.78 cP while NMP has a reported viscosity of 0.92 cP[57]. This increase in solvent viscosity leads to the increase in solution viscosity for solutions made with PolarClean.

a)

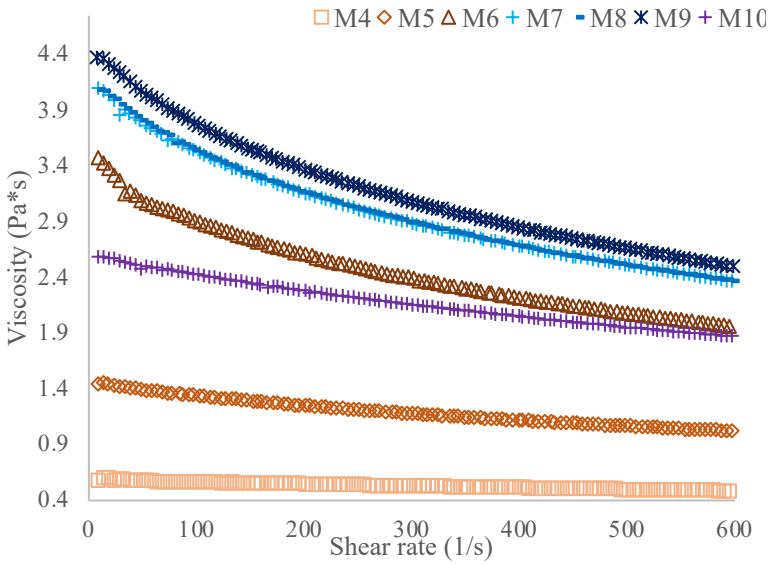


| Solution | Viscosity (Pa*s) |
|---|---|
| M4 | 0.579 ± 0.107 |
| M5 | 1.45 ± 0.413 |
| M6 | 3.47 ± 0.397 |
| M7 | 4.09 ± 0.250 |
| M8 | 4.09 ± 0.323 |
| M9 | 4.37 ± 0.096 |
| M10-13 | 2.58 ± 0.297 |

b)

Figure 3.3 a) M4-10 solution viscosities over a shear rate range of 6-600 1/s b) M4-10 viscosity at shear rate 10 1/s.

Viscosities of solutions containing 12, 15, and 17 wt.% PVDF in NMP are shown below in Figure 3.4. Here it is seen that as PVDF concentration increases, the solution behavior becomes more sheer thinning. This is comparable to literature, whereas the molecular weight of PVDF increased, as did the sheer thinning behavior of the fluid[76]. Viscosity also increased with increasing molecular weight, as seen in Figure 3.4 with increasing concentration. This also mirrors the trend in Figure 3.2b where viscosity increased exponentially with increasing PVDF concentration.

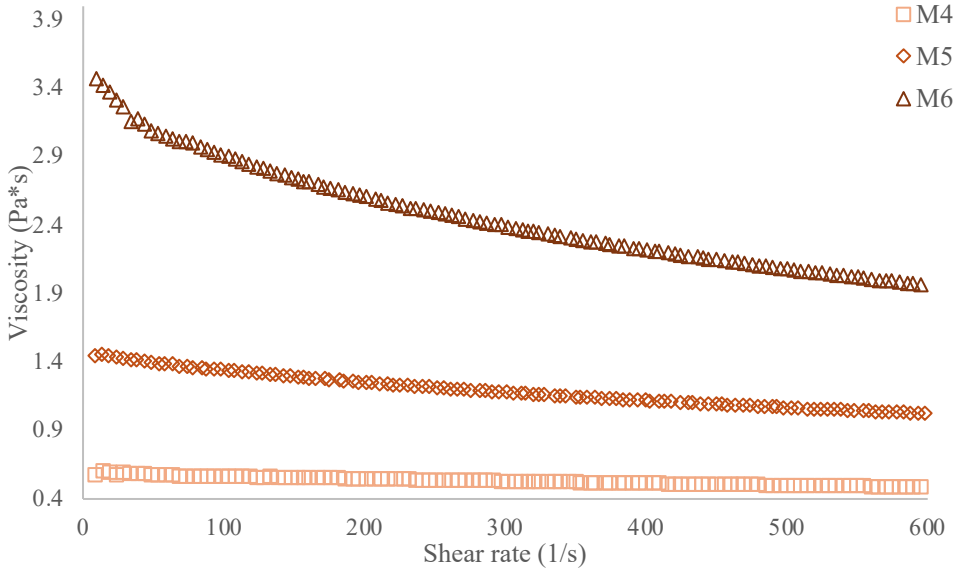


Figure 3.4 Viscosity of solutions with 12 (M4), 15 (M5), and 17 (M6) wt.% PVDF in NMP over a shear rate range of 6-600 1/s.

Viscosities of solutions with 17 wt.% PVDF and varying amounts of PVP from 0-1 wt.% in NMP are plotted in Figure 3.5. The addition of 0.5 wt.% PVP increased viscosity from 3.47 ± 0.397 to 4.09 ± 0.250 Pa*s at a shear rate of 10 1/s. Further increase of PVP content to 0.75 wt.% resulted in a negligible increase in viscosity across the entire shear rate range. Viscosity increased once again to 4.37 ± 0.96 Pa*s when the PVP content was raised to 1 wt.%. The role of PVP as a pore forming additive must be balanced between enhanced demixing due to water solubility and delayed demixing due to increased viscosity.

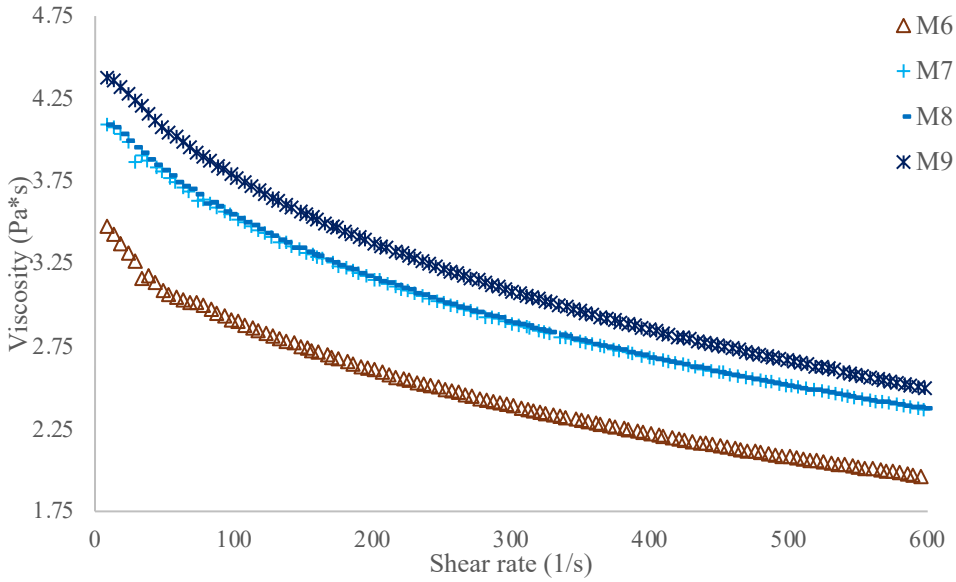


Figure 3.5 Viscosities of solutions containing 17 wt.% PVDF, 0 (M6), 0.5 (M7), 0.75 (M8), and 1 (M9) wt.% PVP in NMP over a shear rate range of 6-600 1/s.

Viscosities of solutions containing 17 wt.% PVDF (M7) or PVDF-HFP (M10) and 0.5 wt.% PVP in NMP are shown in Figure 3.6. The shear thinning behavior and solution viscosity decrease with the inclusion of HFP blocks in the polymer chain. This is likely due to the amorphous nature of HFP which decreases the overall crystallinity of the solution. This viscosity decrease was also observed in literature[77].

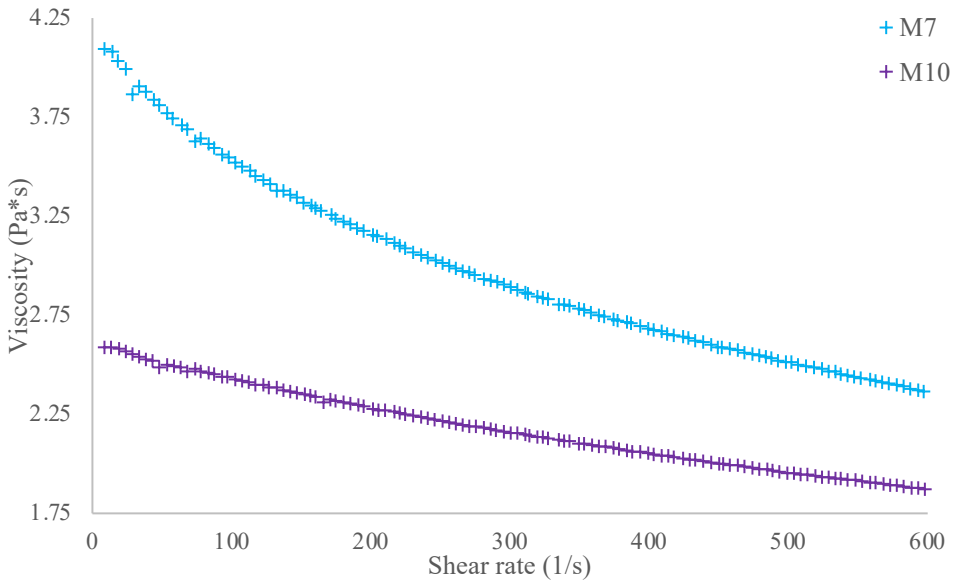


Figure 3.6 Viscosities of solutions containing 17 wt.% PVDF (M7) or PVDF-HFP (M10) and 0.5 wt.% PVP in NMP over a shear rate range of 6-600 1/s.

## 3.4 Membrane structure and morphology

### 3.4.1 Structure

FTIR spectra for membranes M1 - M13 are shown below in Figure 3.7. Figure 3.7a shows the spectra for PVDF membranes prepared with 1 wt.% LiCl and green solvents. The prominent peak ~ 1402 $cm^{-1}$ is associated with the $\alpha$ phase PVDF polymorph. The peaks ~ 1064 and 840 cm-1 are associated with the $\beta$ phase polymorph[61]. The peak at 1184 $cm^{-1}$ can be attributed to $CF_2$ bonds[78]. Figure 3.7b shows the spectra for membranes made from varying concentrations of PVDF in NMP. The same peaks around 1402, 1174, 1071, and 840 $cm^{-1}$ are present, as are the $\alpha$ and $\beta$ PVDF crystalline phases. The peak ~760 $cm^{-1}$ can be associated with rocking vibrations within the matrix[78]. From comparisons between Figure 3.7a and b, it can be deduced that choice of solvent had no real impact on the chemical structure of the membrane, as expected. Figure 3.7b shows no significant change in the surface structure based on polymer concentration. The spectra in Figure 3.7c are for membranes made with varying concentrations of PVP in NMP. As PVP concentration increases, more prominent peaks can be seen ~1663 $cm^{-1}$. These are attributed to vibration of C=O groups, associated with the chemical structure of PVP[78]. This indicates that not all PVP washed out during the phase inversion process at higher concentrations. Figure 3.7d shows the spectra for membranes made from 17 wt.% PVDF-HFP and 0.5 wt.% PVP in NMP. Membranes were cast at decreasing casting speeds. The peaks ~ 765 ($CF_2$ bending), 797 ($CH_2$ rocking), and 975 ($CH_2$ twisting) $cm^{-1}$ are associated with the $\alpha$ phase polymorph of PVDF-HFP. The peaks ~ 840, 874, 1064, 1176, 1279, and 1400 $cm^{-1}$ are associated with

the $\beta$ phase polymorph[47]. The presence of peaks ~1663 $cm^{-1}$ can be attributed to PVP within the matrix.

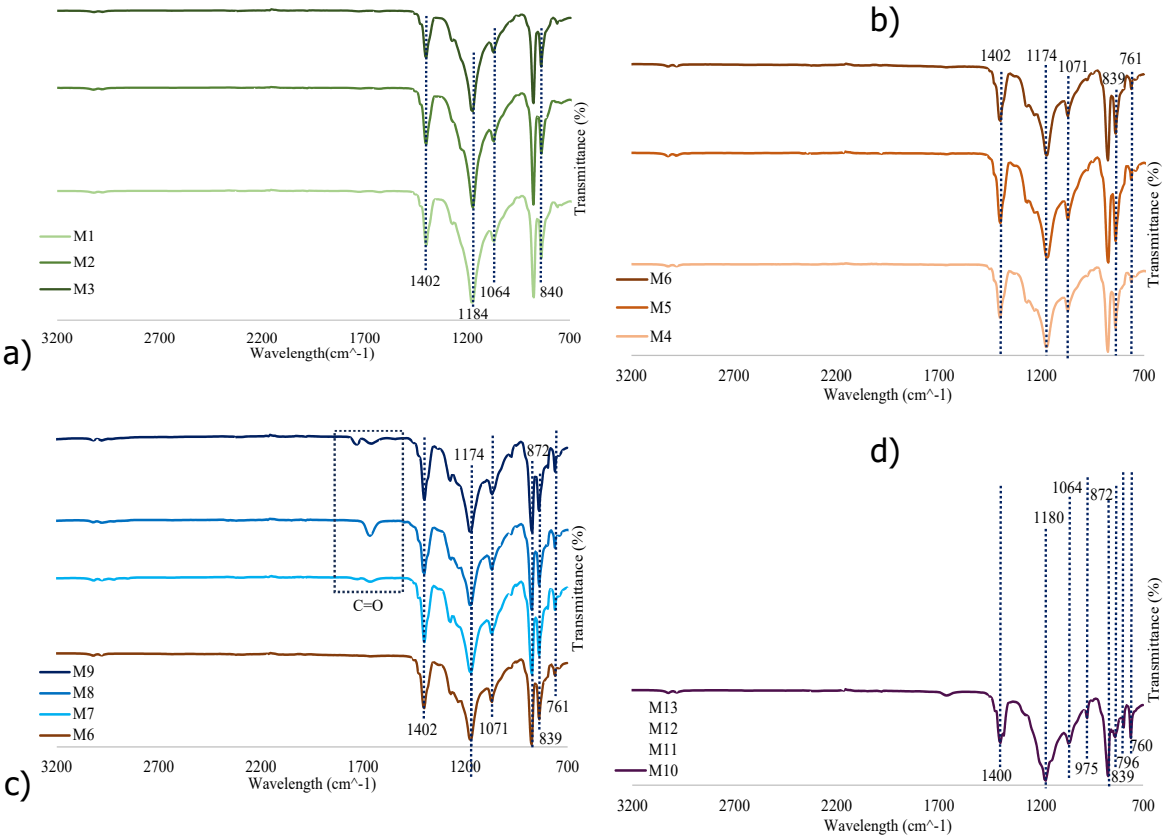


Figure 3.7 FTIR spectra for membranes M1 - M13.

Porosity measured by gas pycnometer is shown below in Figure 3.8 for membranes M4-13. Porosity does not show a linear decrease as polymer concentration increases. This contradicts the thermodynamic and kinetic expectations of the system. A study fabricating PVDF-HFP hollow fiber membranes studied the effect of polymer concentration on void volume fraction[46]. A gradual decrease in void volume fraction was observed as PVDF-HFP concentration increased. The range of polymer concentration studied between M4-6 may not be large enough to resolve a linear decrease in membrane porosity. The dynamics between thermodynamic and kinetic effects must be taken into consideration. At low concentrations, thermodynamics dominate, and instantaneous demixing can occur. The opposite is true at higher concentrations where kinetics dominate and viscosity can work to suppress macrovoid formation, leading to a more sponge-like morphology[46].

With the addition of 0.5 wt.% PVP, membrane porosity decreased from 69.0 ±2.55 % to 53.1 ± 3.24 %. Although PVP is water soluble and should dissolve during phase inversion, FTIR results show bonds attributed to PVP within the polymer matrix. With higher concentrations of PVP at 0.75 and 1 wt.% porosity increased to 84.1 ± 1.00 and 86.0 ± 1.35 %. Other studies exploring the influence of additives to PVDF

membranes often use higher concentrations, between 2.5 and 7 wt.%[53]. Low concentrations of PVP, like 0.5 wt.%, may have become trapped within the solution, inhibiting its pore forming properties.

The inclusion of HFP between M7 and M10 lead to an increase in porosity to 87.3 ± 1.39 %. This is opposite of trends found in literature where porosity decreases with the inclusion of HFP[77]. However, this porosity increase may be a result of decreased viscosity, as shown in Figure 3.6. Porosity decreases slightly as casting speed decreases. Another study exploring the effect of shear rate on membrane formation found a slight difference on effective porosity[42]. This difference was overall negligible; however, the induced shear acted to orient the selective skin layer which enhanced separation performance.

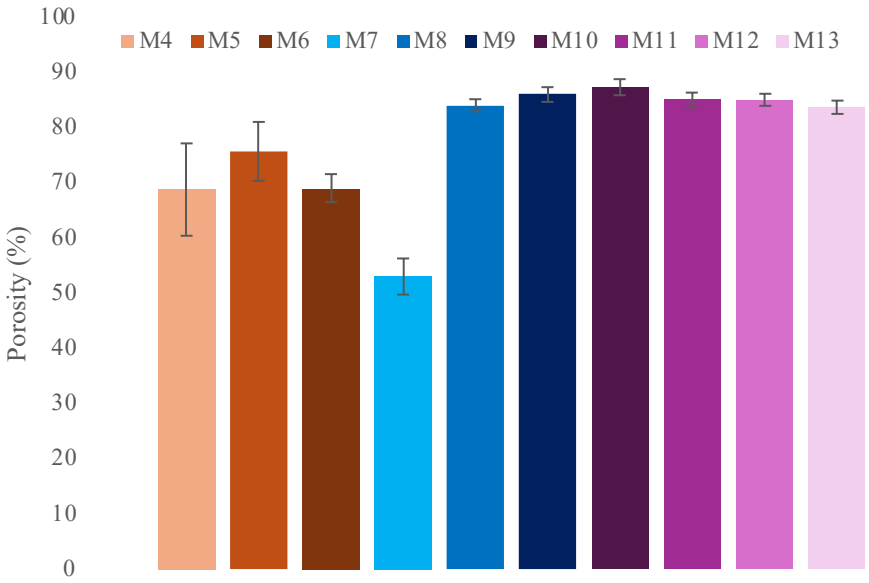


Figure 3.8 Porosity measured by gas pycnometer for membranes M4 - M13.

The Young's modulus of each membrane is plotted below in Figure 3.9. As previously mentioned, M1 was extremely fragile during handling and has a significantly lower modulus than any other membrane tested. It is extremely thin cross section likely contributes to the lack of mechanical strength. M3, although fabricated with green solvents, had a modulus within a similar range to those made from NMP. This can be attributed to the extremely dense cross-sectional morphology. M6 had a modulus outside the range of other membranes tested. This higher strength could be due to the increased polymer concentration and lack of additive, therefore; higher chances of developing a more crystalline matrix. The addition of a pore forming additive greatly decreased mechanical strength; however, there was a negligible difference upon increasing the concentration of PVP. The influence of casting conditions was found to have a significant impact on mechanical strength. M11, cast at a shear rate of 466.7 1/s had a higher modulus than membranes cast at lower and higher shear rates.

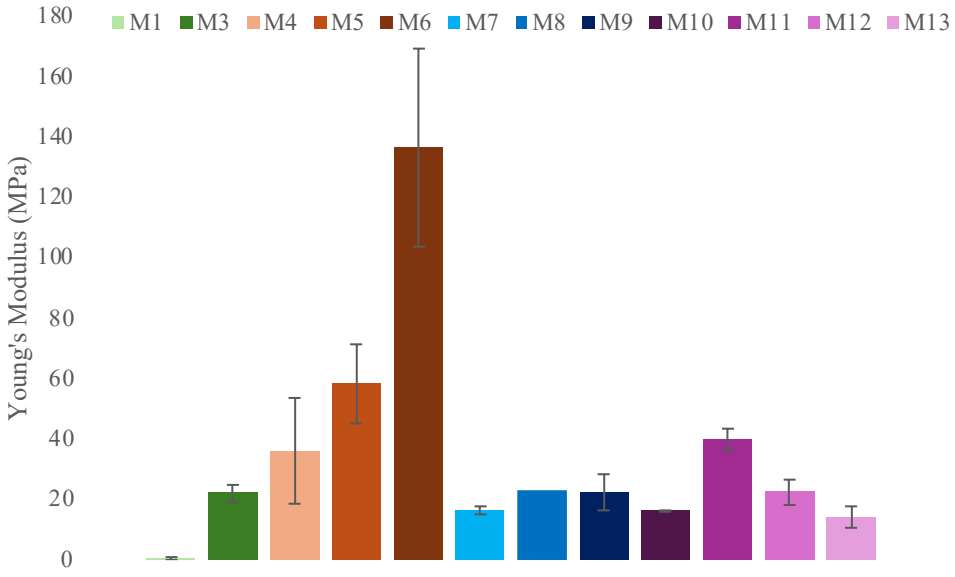


Figure 3.9 Young's modulus for membranes M1, M3 - M13.

The contact angle of a droplet of DI water on the dried membrane surface for membranes M1-13 is plotted below in Figure 3.10. A contact angle greater than or equal to 90 ºC corresponds with a hydrophobic surface. M3 showed the highest contact angle and highest standard deviation, indicating a hydrophobic surface and unstable interaction with the water droplet as a result. Using NMP as a solvent decreased the contact angle compared with green solvents and increasing polymer concentration increased contact angle slightly. This is expected due to PVDF's hydrophobic nature. The addition of PVP lowered contact angle. PVP is hydrophobic and can help to decrease contact angle when present. The surface roughness observed on the cross-sectional morphology of M7 could also contribute to a lower contact angle by disturbing the interaction between the surface and the water droplet. However, hydrophobicity did not increase with increasing concentration of PVP. There was an increase in hydrophobicity when using PVDF-HFP, as expected due to increased fluorine content. Casting speed influenced contact angle in a similar trend to mechanical strength, indicating more polymer chain alignment along the surface due to induced shear.

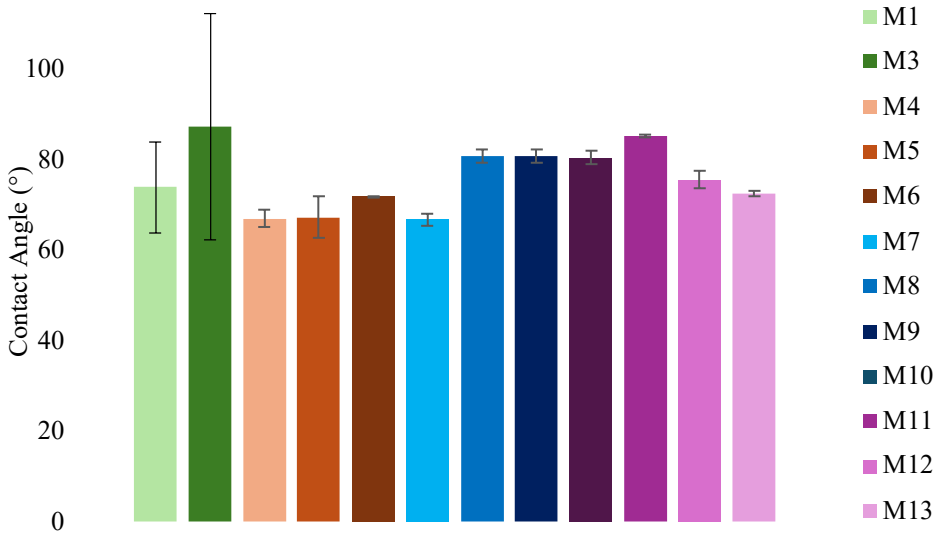


Figure 3.10 Contact angle of a 12-microliter droplet of DI water on membrane surface for M1, M3 - M13.

### 3.4.2 Morphology

Figure 3.11 shows SEM images for membranes a/b) M1 and c/d) M3, 15 wt.% PVDF and 1 wt.% LiCl in green solvents, at 500 and 100x magnification. Both membranes from green solvents were extremely fragile when handling, which could be attributed to their thinness. This fragility made cross-sectional imaging especially difficult for M1. Cross-sectional images of M3 show a very dense, sponge-like morphology, as expected when utilizing green solvents[66]. This morphology is also expected from more viscous solutions, like those shown in Figure 3.2.

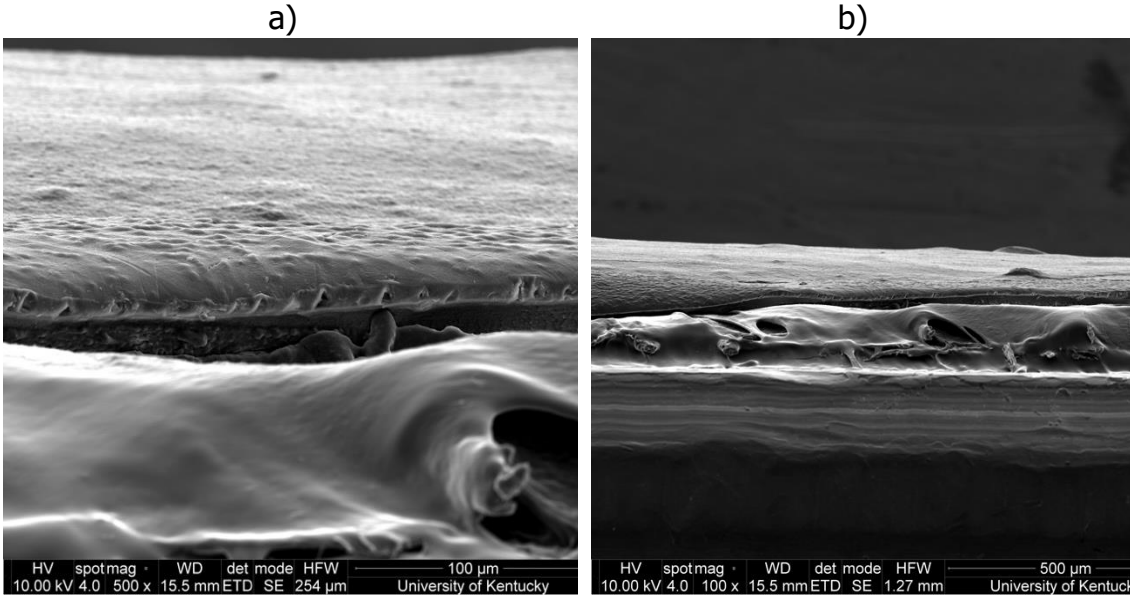

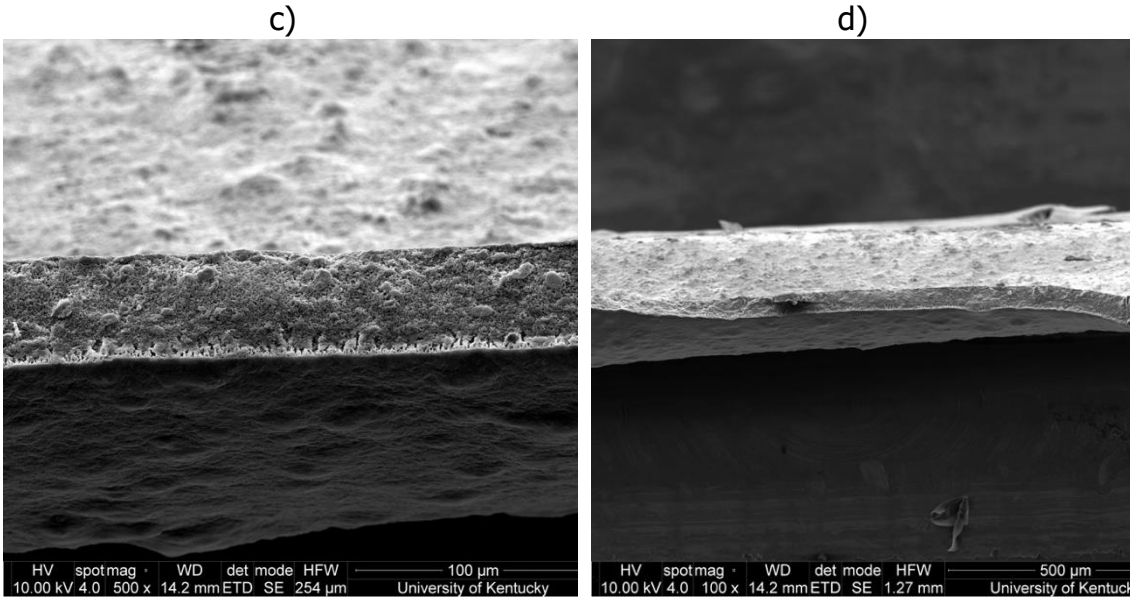


Figure 3.11 SEM images for a, b) M1 and c, d) M3 at 500x and 100x magnification.

SEM images of membranes M4, M5 and M6 at 500 and 100x magnification are shown in Figure 3.12 a-f. As polymer concentration increases, macrovoid volume appears to decrease, leading to a relatively denser morphology. This also leads to an increase in pore connectivity throughout the thickness of the polymer matrix. The presence of finger-like macrovoids, characteristic of instantaneous demixing, is evident in comparison with Figure 3.9. Membranes made with green solvents present a very different morphology from those made with NMP as the solvent.

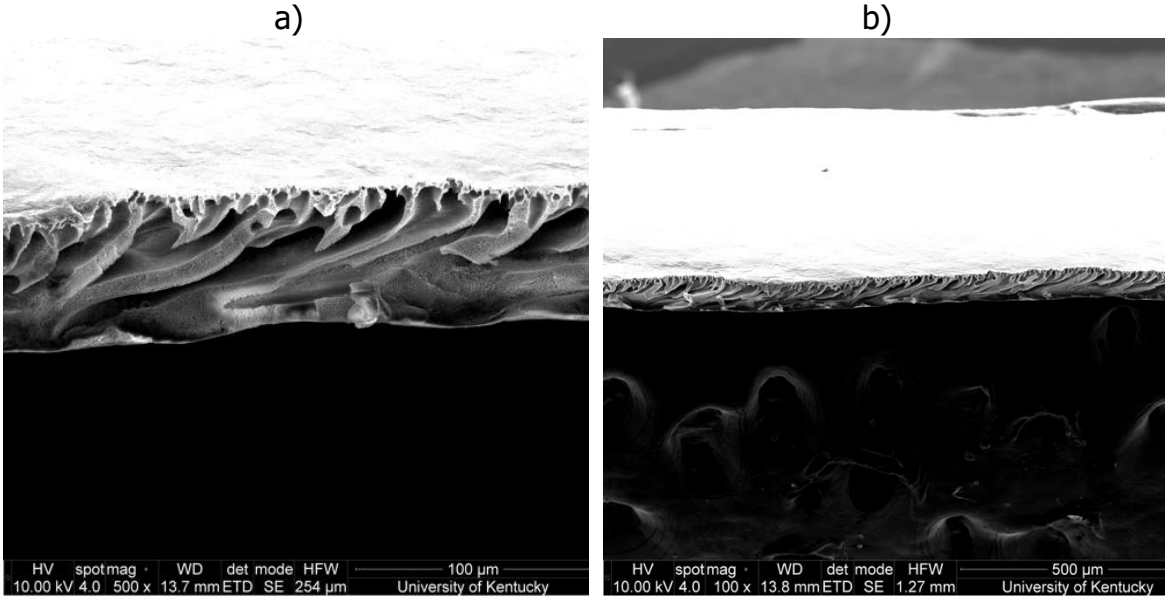

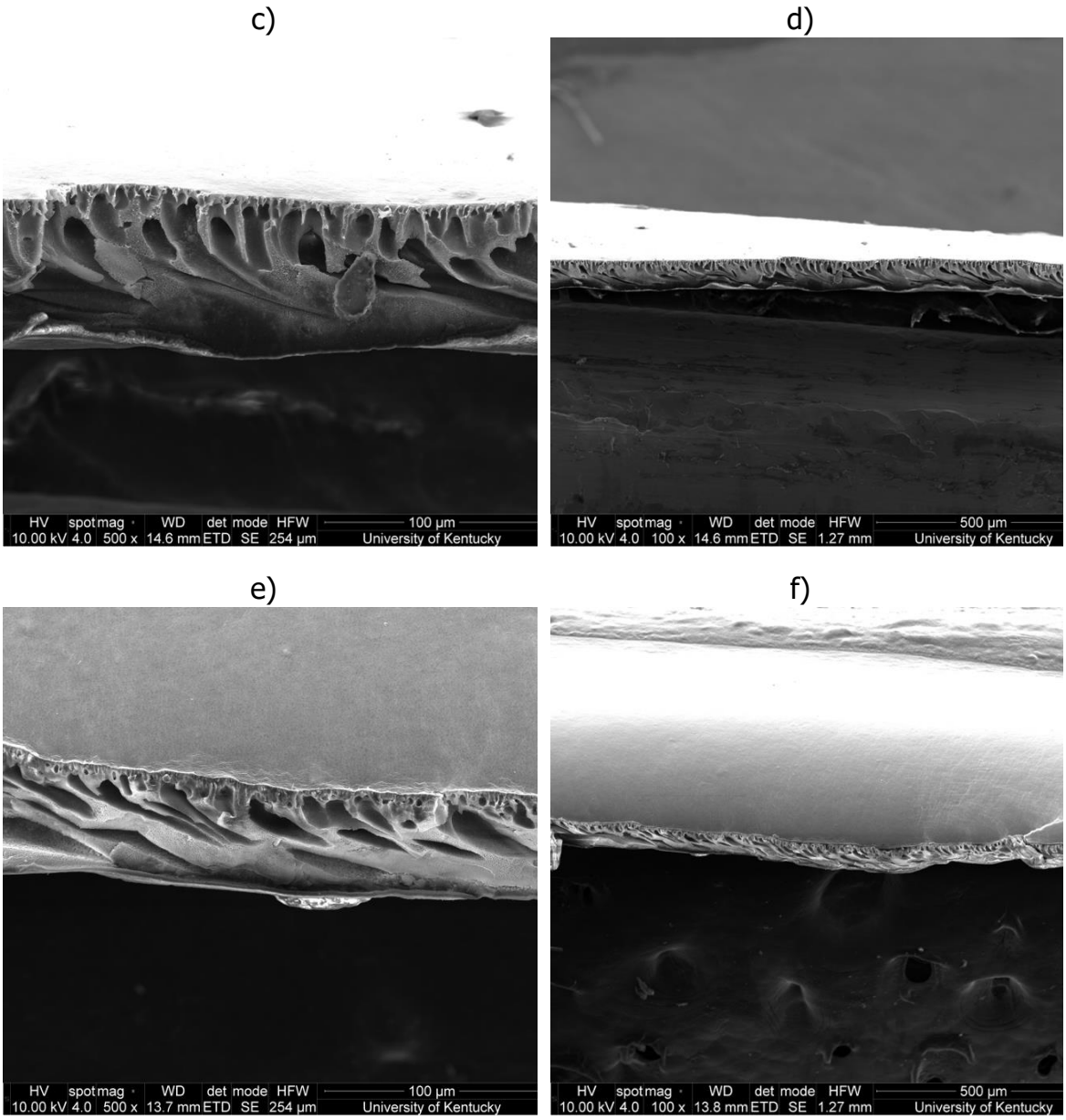


Figure 3.12 SEM images for a, b) M4, c, d) M5, and e, f) M6 at 500x and 100x magnification.

SEM images of membranes M7, M8, and M9 are displayed in Figure 3.13. These images show the same finger-like macrovoids as membranes without any pore forming additive. As PVP concentration increases, these macrovoids become accentuated and extended throughout the membrane thickness. This can be seen most clearly in Figure 3.11e and f when PVP concentration in the solution was increased to 1 wt.%. The increased roughness in Figure 3.11 3a, in conjunction with a lower porosity and FTIR results, suggest the concentration of PVP at 0.5 wt.% was not sufficient to overcome kinetic barriers and act as a pore former.

a)

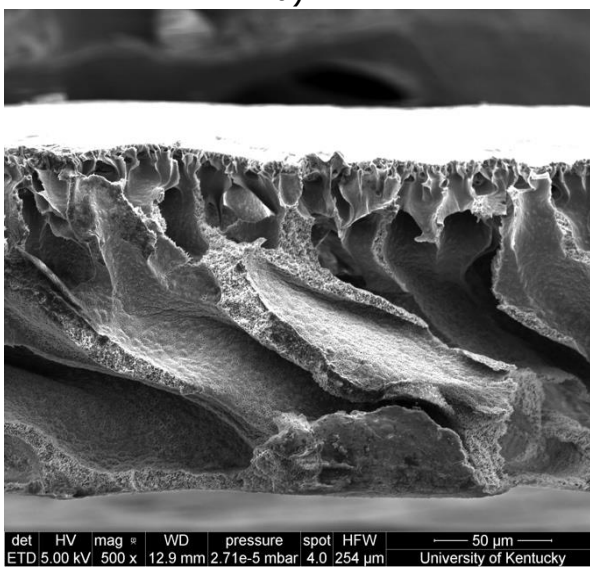
det HV mag WD pressure spot HFW 50 µm
ETD 5.00 kV 500 x 12.9 mm 2.71e-5 mbar 4.0 254 µm University of Kentucky

b)

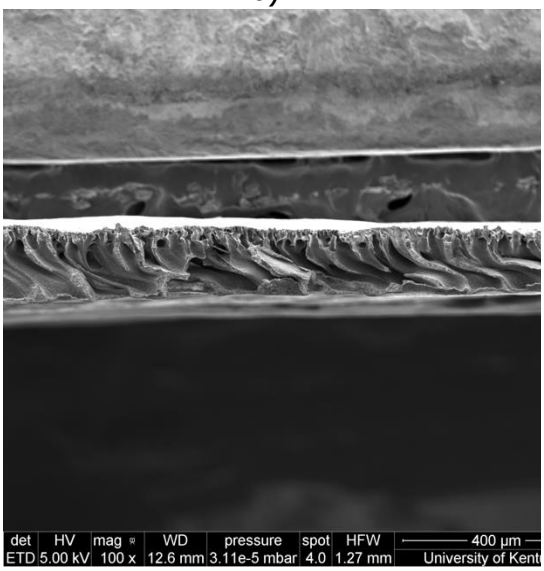
det HV mag WD pressure spot HFW 400 µm
ETD 5.00 kV 100 x 12.6 mm 3.11e-5 mbar 4.0 1.27 mm University of Kent

c)

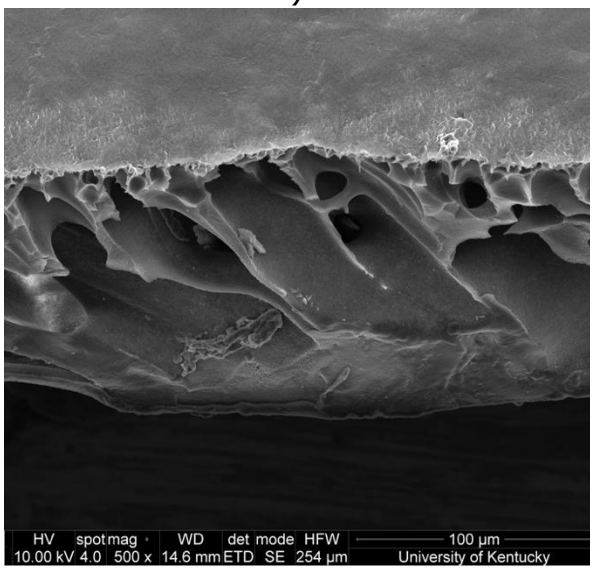
HV spot mag WD det mode HFW 100 µm
10.00 kV 4.0 500 x 14.6 mm ETD SE 254 µm University of Kentucky

d)

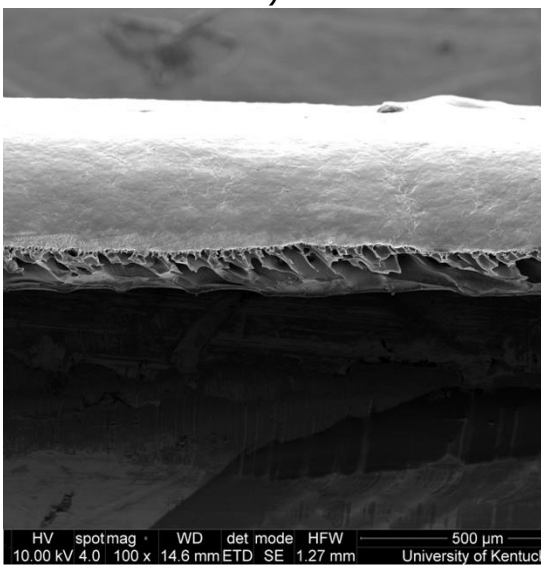
HV spot mag WD det mode HFW 500 µm
10.00 kV 4.0 100 x 14.6 mm ETD SE 1.27 mm University of Kentuc

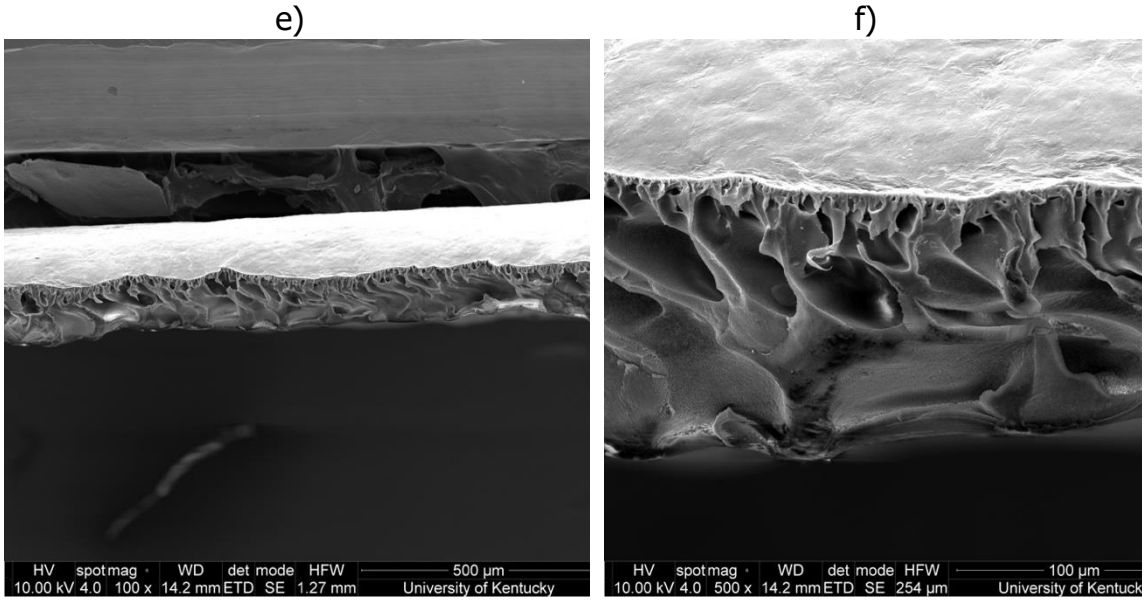


Figure 3.13 SEM images of membranes a, b) M7, c, d) M8, and e, f) M9 at 500x and 100x magnification.

Figure 3.14 shows SEM images of membranes M10, M11, M12, and M13. There is a clear morphological difference in M12. The pore structure of this membrane appears to have formed with very little slant in comparison to all other membranes with macrovoids shown here, forming more spherically shaped voids instead of finger-like. This indicates the casting speed during doctor blade extrusion of M12 did not induce sufficient shear to order the polymer chains on the surface. Thus, the tortuosity of the pore structure is influenced by casting speed.

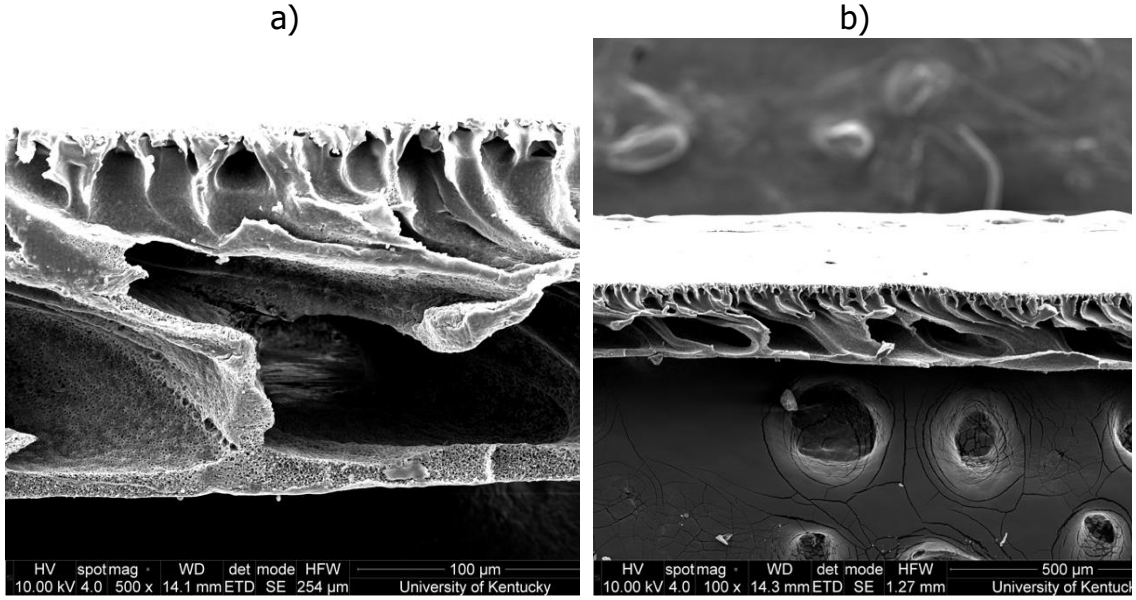

c)

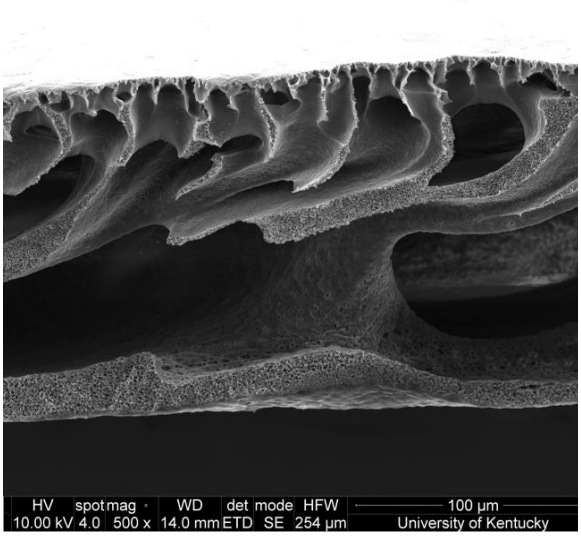
HV spot mag WD det mode HFW
10.00 kV 4.0 500 x 14.0 mm ETD SE 254 µm
100 µm
University of Kentucky

d)

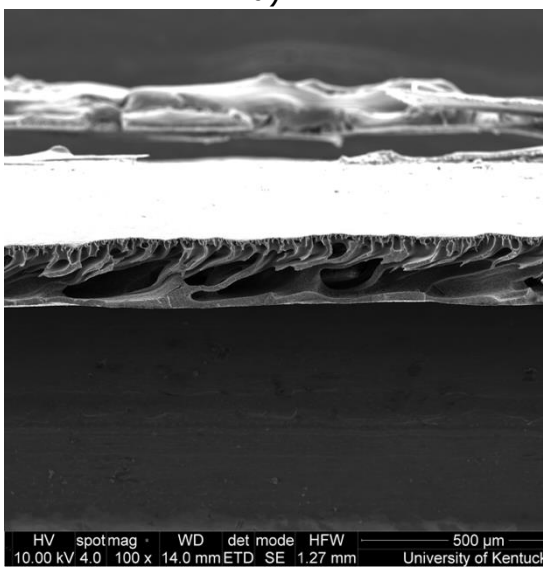
HV spot mag WD det mode HFW
10.00 kV 4.0 100 x 14.0 mm ETD SE 1.27 mm
500 µm
University of Kentuc

e)

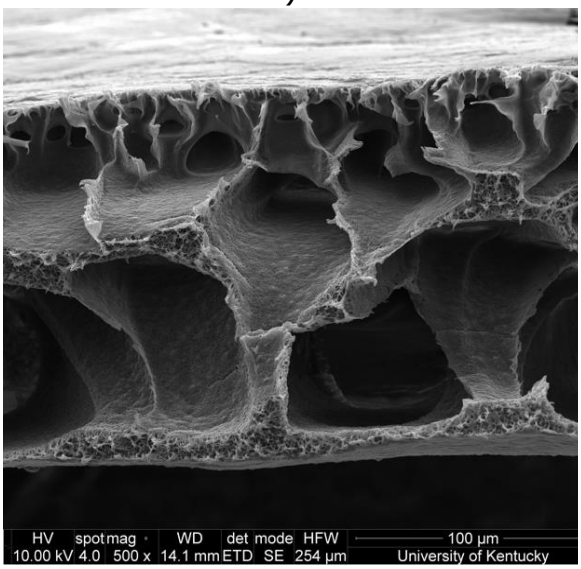
HV spot mag WD det mode HFW
10.00 kV 4.0 500 x 14.1 mm ETD SE 254 µm
100 µm
University of Kentucky

f)

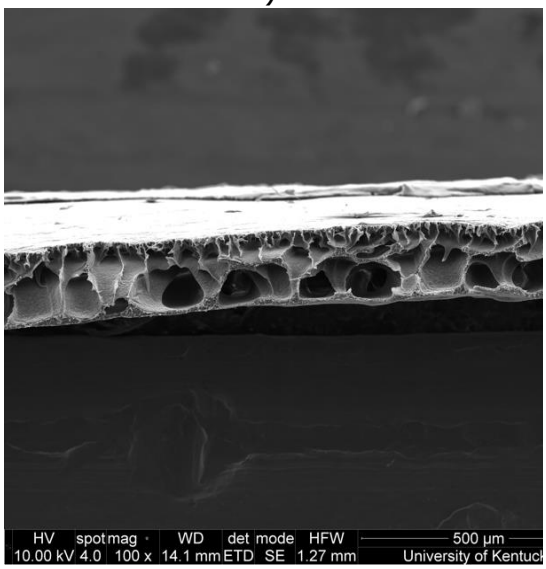
HV spot mag WD det mode HFW
10.00 kV 4.0 100 x 14.1 mm ETD SE 1.27 mm
500 µm
University of Kentuc

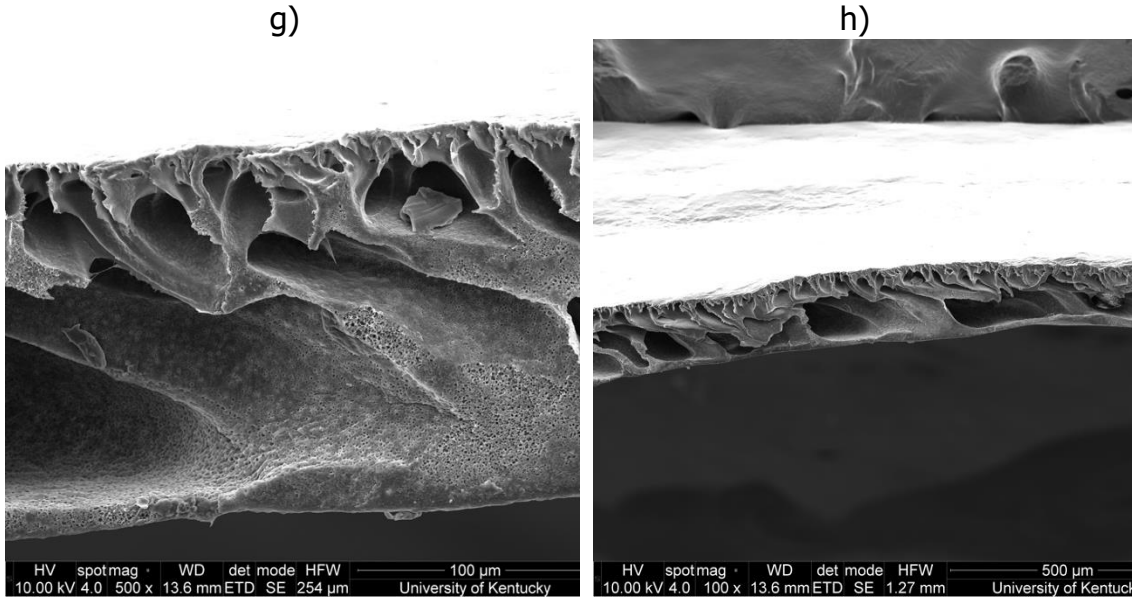


Figure 3.14 SEM images of a, b) M10, c, d) M11, e, f) M12, and g, h) M13 in order of decreasing casting speed, at 500x and 100x magnification.

## 3.5 Operation and performance

Filtration results for membranes M1 and M3 are displayed below in Figure 3.15. The results demonstrate that the choice of casting solvent significantly impacted membrane permeability. Membranes made with PolarClean (M1) had an average pure water permeability of 145 ± 44.6 LMH/bar and membranes made with the cosolvent mixture (M3) had an average of 57.3 ± 6.94 LMH/bar. The higher permeability and standard deviation results from M1 are likely due to low mechanical strength, as seen in Figure 3.9. It is likely that this membrane ruptured during performance testing under 4.137 bar. This would explain the inconsistent separation performance seen in Figure 3.15b, with an average rejection of 12.7 ± 8.55%. Similar results were observed when using PolarClean as a lone solvent for PSf and led to pore collapse during filtration[66]. The polymer matrix comprising M1 was not robust enough to withstand performance operation parameters. The reduced permeability when using a 3:1 PolarClean to GVL cosolvent can be attributed to the very dense, sponge-like morphology in Figure 3.11c and d. PolarClean tends to form macrovoids in the membrane morphology, while GVL produces a sponge-like morphology[61, 64]. The incorporation of GVL, along with the inherent increased viscosity of solutions prepared with PolarClean, led to the suppression of macrovoid formation. The higher hydrophobicity of M3 (Figure 3.10) likely led to the inconsistent separation performance, with an average rejection of 20.1 ± 13.5%. With such a dense morphology, rejection is expected to be relatively high; however, highly hydrophobic surfaces in UF and MF applications cause decreased efficiency and increased fouling potential.

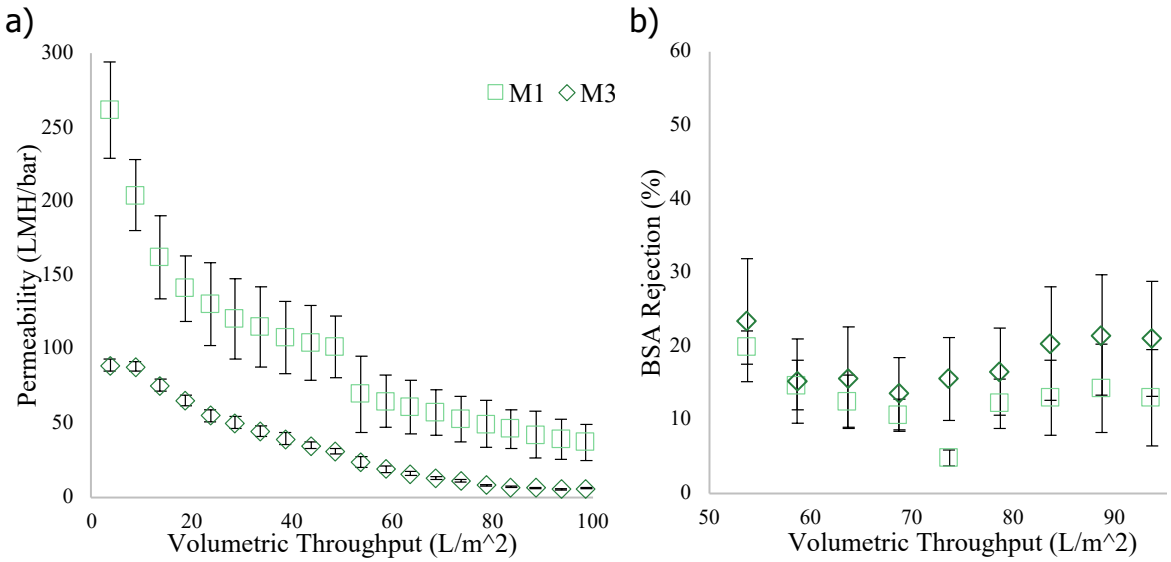


Figure 3.15 a) Permeability and b) BSA rejection results for membranes M1 and M3.

Performance results for membranes M4, M5, and M6 are shown below in Figure 3.16. Permeability results directly mirror porosity results for each membrane, as seen in Figure 3.8, with M5 having the highest porosity and permeability at 395 ± 46.1 LMH/bar. M6 had the lowest porosity and permeability at 57.9 ± 16.5 LMH/bar. M4 had a sharp decline in permeability as volumetric throughput increased. This can be attributed to the reduced mechanical strength, as seen in Figure 3.9. This indicates that the pore structure was at risk for collapsing under operating pressures and explains the decrease in BSA rejection as volumetric throughput increased in Figure 3.16b. A collapsed pore structure, or very low surface porosity, can also lead to instantaneous fouling. This might explain the sharp decrease in permeability between pure water and BSA solution filtration at 50 $L/m^2$. The very low permeability and rejection of M6 can be attributed to higher hydrophobicity due to increased polymer concentration. This higher concentration also led to increased mechanical strength, indicating a higher degree of crystallinity and lower porosity.

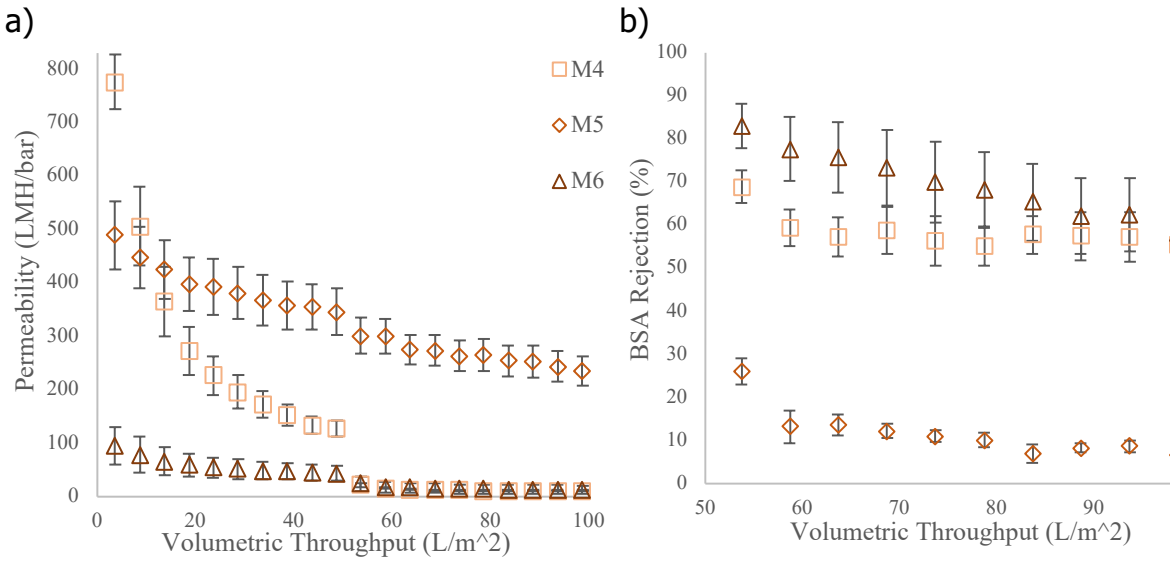


Figure 3.16 a) Permeability and b) BSA rejection results for membranes M4, M5, and M6.

Filtration results for M7, M8, and M9 in comparison with M6 are shown in Figure 3.17. The addition of PVP to the polymer solution significantly permeability. Specifically, pure water permeability increased an average of 408 ± 145 LMH/bar with the addition of 0.5 wt.% PVP, 643 ± 243 LMH/bar with 0.75 wt.% PVP, and 570 ± 142 LMH/bar with 1 wt.% PVP at the end of precompaction. This indicates that PVP effectively promotes pore formation in the membrane, as confirmed by SEM images in Figure 3.13. This increased porosity led to decreased BSA rejection for all membranes containing PVP compared to those without. This reduced selectivity of membranes with 1 wt.% PVP indicates that excessive porosity can negatively impact BSA rejection. Additionally, membranes containing PVP exhibited greater surface roughness variability compared to those without PVP. This variability increased with higher PVP concentration, suggesting that a PVP concentration between 0.5-0.75 wt.% is optimal.

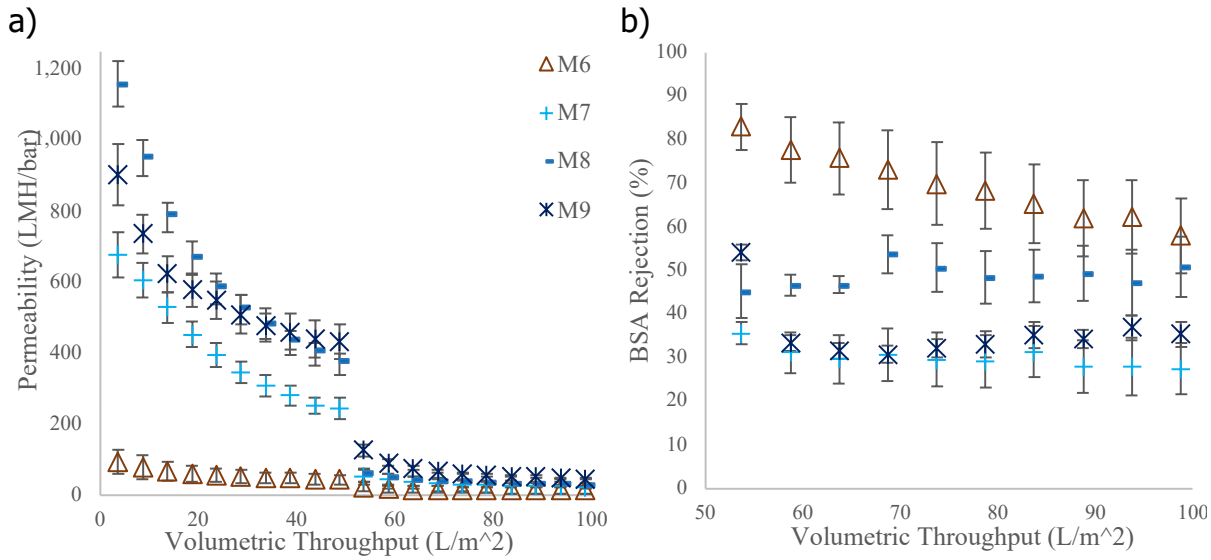


Figure 3.17 a) Permeability and b) BSA rejection results for membranes M6, M7, M8, and M9.

Permeability and rejection results for M10 in comparison with M7 are displayed in Figure 3.5. The inclusion of a copolymer in the dope solution decreased pure water permeability from 243 ± 85.9 LMH/bar to 96.8 ± 42.8 LMH/bar at the end of precompaction. However, differences in permeability during filtration were negligible, as evidenced by minimal differences in rejection between the two membrane compositions. The decrease in permeability is likely due to an increase in hydrophobicity, as seen in Figure 3.10.

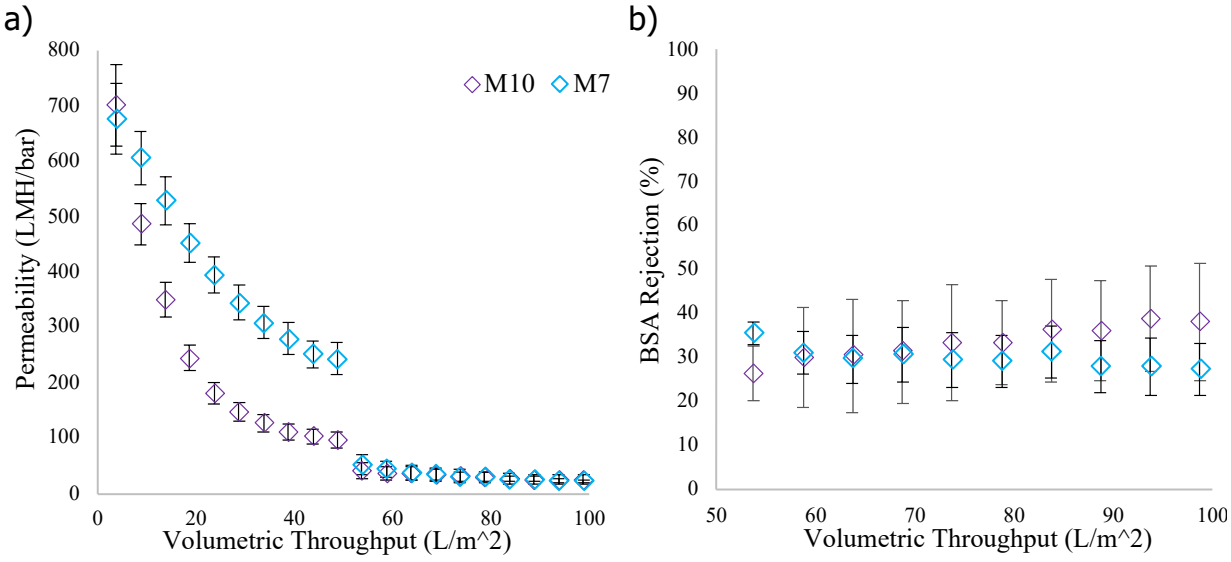


Figure 3.18 a) Permeability and b) BSA rejection results for M7 and M10.

To further optimize membrane performance, the influence of casting conditions was explored. PVDF-HFP membranes were cast at five different casting speeds on an automatic film coater. The casting speeds and corresponding shear rates, calculated using Equation 10, are listed in Table 3.4. Membrane thickness was considered as the coating

gap during casting and kept constant at 250 $\mu$m, resulting in shear rate decreasing linearly with casting speed.

TABLE 3.2 CASTING SPEEDS (CM/SEC) AND CORRESPONDING INDUCED SHEAR RATES USING EQ. 10.

| Membrane | Casting Speed (cm/min) | Shear rate ($s^{-1}$) |
|---|---|---|
| M10 | 900 | 600 |
| M11 | 700 | 467 |
| M12 | 500 | 333 |
| M13 | 300 | 200 |

Filtration results for membranes M10, M11, M12, M13 are displayed in Figure 3.19. The permeability results show a significant difference in pure water permeability for M11, which was cast at under a shear rate of 467 1/s. This increase, followed by a rapid decrease in permeability as shear increases, indicates the critical shear for this system has been reached. Additional shear, such as 600 1/s, results in a decrease in permeability and rejection. Similarly, shear rates below 466.7 1/s do not induce enough of a structured morphology to allow for optimized permeability and selectivity. This is supported by similar trends in contact angle and mechanical strength.

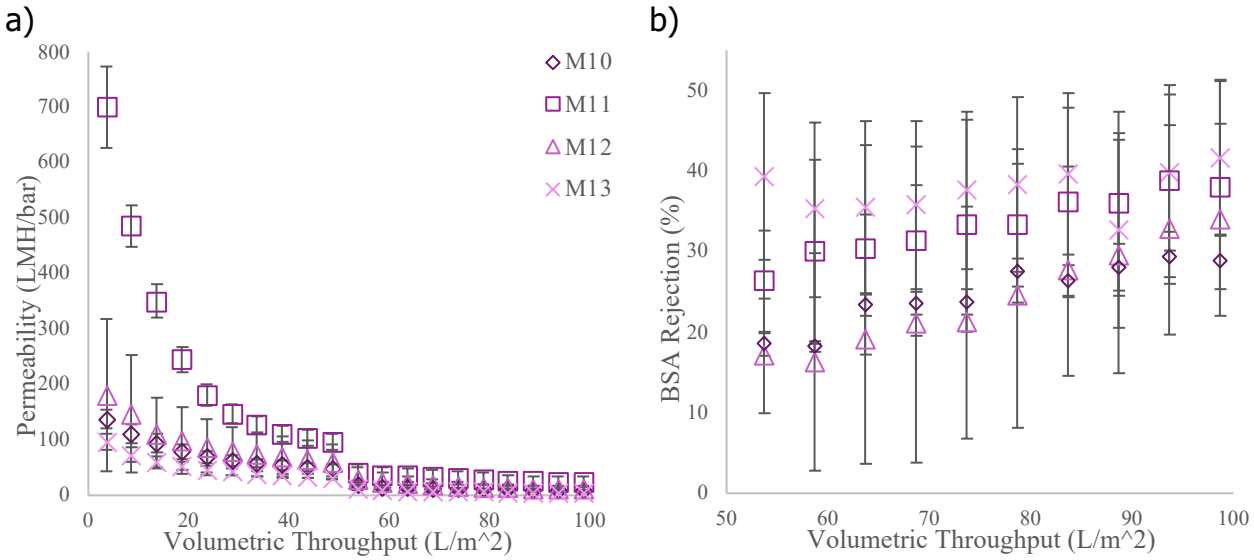


Figure 3.19 a) Permeability and b) BSA rejection results for membranes M10, M11, M12, and M13.

# CHAPTER 4. CONCLUSIONS AND FUTURE WORK

## 4.1 Conclusions

The merits of membranes for contaminant removal of water have been discussed. The complicated nature of nonsolvent induced phase separation for each individual system must be taken into consideration. This work explored the influence of various solvents, additives, and casting conditions on the performance of PVDF-based membranes. The choice of casting solvent significantly impacts membrane structure and performance. Green solvents produced membranes with lower mechanical strength and porosity than those fabricated with NMP as the casting solvent. Solutions made with green solvents were also significantly more viscous than those without and resulted in a very dense sponge-like morphology. The addition of polyvinylpyrrolidone (PVP) into the polymer solution significantly enhanced pure water permeability, however; large macrovoids in the membrane structure at higher PVP concentrations led to a decrease in selectivity. A PVP concentration range of 0.5-0.75 wt.% was identified as ideal to balance thermodynamic and kinetic forces. The inclusion of PVDF-HFP copolymer decreased permeability due to increased hydrophobicity, attributed to the additional fluorine content. The copolymer produced a more thermodynamically stable solution, as evidenced by the shift in cloud point curve towards the nonsolvent axis. Varying the casting speed demonstrated that a critical shear rate (466.6 1/s) optimized permeability and selectivity. Shear rates above or below this threshold resulted in decreased performance and lower mechanical strength. Overall, this work highlights the complex interplay between solvent choice, polymer concentration, additives, and casting conditions in determining membrane performance. These findings provide valuable insights for the design and optimization of PVDF-based membranes for various filtration applications.

## 4.2 Future Work

While the current study provides significant insights into the optimization of PVDF-based membranes, several avenues for future research could further enhance our understanding and performance of these membranes. Key areas for future work include testing other model particles, exploring the impact of dissolution temperature, and other additives. Investigating the performance if PVDF membrane against a broader range of model particles, including different sizes and chemical properties, can provide a more comprehensive evaluation of membrane selectivity and fouling behavior. Conducting tests with real-world water samples containing multiple contaminants will help assess the membrane's practical applicability and robustness. Investigating the effect of different dissolution temperatures of the solubility and stability of PVDF and PVDF-HFP solutions can provide deeper insights into the phase inversion process and resultant membrane. Analyzing how dissolution temperature influences membrane permeability, selectivity, and mechanical properties will help identity optimal processing conditions for various

applications. Beyond PVP, exploring other water-soluble pore-forming agents such as PEG or surfactants could lead to further enhancements in membrane structure and performance. The impact of these agents on pore size distribution and surface roughness will be critical to study. Incorporating hydrophilic additives or surface modification treatment techniques could enhance water flux and reduce fouling propensity, further improving membrane efficiency. By addressing these areas, further research can build on the current findings to develop highly efficient, robust, and versatile PVDF-based membranes for a wide range of filtration applications.

REFERENCES


[1] M. M. Mekonnen and A. Y. Hoekstra, "Four billion people facing severe water scarcity," *Science Advances,* vol. 2, no. 2, p. e1500323, 2016, doi: 10.1126/sciadv.1500323.

[2] W. A. Jury and H. J. Vaux, "The Emerging Global Water Crisis: Managing Scarcity and Conflict Between Water Users," in *Advances in Agronomy*, vol. 95: Academic Press, 2007, pp. 1-76.

[3] U. N. D. o. E. a. S. Affairs, "The Sustainable Development Goals Report 2023: Special Edition - July 2023," UN DESA, New York, USA, 2023. [Online]. Available: https://unstats.un.org/sdgs/report/2023/

[4] S. Sharma and A. Bhattacharya, "Drinking water contamination and treatment techniques," *Applied Water Science,* vol. 7, no. 3, pp. 1043-1067, 2017, doi: 10.1007/s13201-016-0455-7.

[5] J. Bratby, *Coagulation and flocculation in water and wastewater treatment*. IWA publishing, 2016.

[6] S. A. Snyder, P. Westerhoff, Y. Yoon, and D. L. Sedlak, "Pharmaceuticals, personal care products, and endocrine disruptors in water: implications for the water industry," *Environmental engineering science,* vol. 20, no. 5, pp. 449-469, 2003.

[7] U. Von Gunten, "Ozonation of drinking water: Part I. Oxidation kinetics and product formation," *Water research,* vol. 37, no. 7, pp. 1443-1467, 2003.

[8] M. A. Shannon, P. W. Bohn, M. Elimelech, J. G. Georgiadis, B. J. Marinas, and A. M. Mayes, "Science and technology for water purification in the coming decades," *Nature,* vol. 452, no. 7185, pp. 301-310, 2008.

[9] D. M. Warsinger *et al.*, "A review of polymeric membranes and processes for potable water reuse," *Progress in Polymer Science,* vol. 81, pp. 209-237, 2018, doi: 10.1016/j.progpolymsci.2018.01.004.

[10] T. D. Appleman *et al.*, "Treatment of poly-and perfluoroalkyl substances in US full-scale water treatment systems," *Water research,* vol. 51, pp. 246-255, 2014.

[11] V. Abetz, T. Brinkmann, and M. Sözbilir, "Fabrication and function of polymer membranes," *Chemistry Teacher International,* vol. 3, no. 2, pp. 141-154, 2021, doi: 10.1515/cti-2020-0023.

[12] A. Fane, W. Xi, and W. Rong, "Membrane filtration processes and fouling," in *Interface Science and Technology*, vol. 10: Elsevier, 2006, pp. 109-132.

[13] C. Charcosset, "Microfiltration," *Membrane processes in biotechnology and pharmaceutics,* pp. 101-141, 2012.

[14] A. Sagle and B. Freeman, "Fundamentals of membranes for water treatment," *The future of desalination in Texas,* vol. 2, no. 363, p. 137, 2004.

[15] D. R. Lloyd, K. E. Kinzer, and H. S. Tseng, "Microporous membrane formation via thermally induced phase separation. I. Solid-liquid phase separation," *Journal of Membrane Science,* vol. 52, no. 3, pp. 239-261, 1990/09/15/ 1990, doi: https://doi.org/10.1016/S0376-7388(00)85130-3.

[16] M. Mulder, *Basic principles of membrane technology*. Springer science & business media, 2012.

[17] I. Wenten, "Mechanisms and control of fouling in crossflow microfiltration," *Filtration & separation,* vol. 32, no. 3, pp. 252-253, 1995.

[18] G. R. Guillen, Y. Pan, M. Li, and E. M. V. Hoek, "Preparation and Characterization of Membranes Formed by Nonsolvent Induced Phase Separation: A Review," *Industrial & Engineering Chemistry Research,* vol. 50, no. 7, pp. 3798-3817, 2011, doi: 10.1021/ie101928r.

[19] X. Dong, D. Lu, T. A. Harris, and I. C. Escobar, "Polymers and solvents used in membrane fabrication: a review focusing on sustainable membrane development," *Membranes,* vol. 11, no. 5, p. 309, 2021.

[20] A. K. Hołda and I. F. J. Vankelecom, "Understanding and guiding the phase inversion process for synthesis of solvent resistant nanofiltration membranes," *Journal of Applied Polymer Science,* vol. 132, no. 27, pp. n/a-n/a, 2015, doi: 10.1002/app.42130.

[21] H. Strathmann and K. Kock, "The formation mechanism of phase inversion membranes," *Desalination,* vol. 21, no. 3, pp. 241-255, 1977/09/01/ 1977, doi: https://doi.org/10.1016/S0011-9164(00)88244-2.

[22] K. Kimmerle and H. Strathmann, "Analysis of the structure-determining process of phase inversion membranes," *Desalination,* vol. 79, no. 2, pp. 283-302, 1990/12/01/ 1990, doi: https://doi.org/10.1016/0011-9164(90)85012-Y.

[23] C. A. Smolders, A. J. Reuvers, R. M. Boom, and I. M. Wienk, "Microstructures in phase-inversion membranes. Part 1. Formation of macrovoids," *Journal of Membrane Science,* vol. 73, no. 2-3, pp. 259-275, 1992, doi: 10.1016/0376-7388(92)80134-6.

[24] H. Strathmann, "Membrane separation processes," *Journal of Membrane Science,* vol. 9, no. 1, pp. 121-189, 1981/01/01/ 1981, doi: https://doi.org/10.1016/S0376-7388(00)85121-2.

[25] M. L. Yeow, Y. T. Liu, and K. Li, "Isothermal phase diagrams and phase-inversion behavior of poly(vinylidene fluoride)/solvents/additives/water systems," *Journal of Applied Polymer Science,* vol. 90, no. 8, pp. 2150-2155, 2003, doi: 10.1002/app.12846.

[26] C. Cohen, G. Tanny, and S. Prager, "Diffusion-controlled formation of porous structures in ternary polymer systems," *Journal of Polymer Science: Polymer Physics Edition,* vol. 17, no. 3, pp. 477-489, 1979.

[27] P. Radovanovic, S. W. Thiel, and S.-T. Hwang, "Formation of asymmetric polysulfone membranes by immersion precipitation. Part I. Modelling mass transport during gelation," *Journal of Membrane Science,* vol. 65, no. 3, pp. 213-229, 1992/01/15/ 1992, doi: https://doi.org/10.1016/0376-7388(92)87024-R.

[28] C. M. Hansen, "The three dimensional solubility parameter," *Danish Technical: Copenhagen,* vol. 14, 1967.

[29] M. Díaz de los Ríos and E. Hernández Ramos, "Determination of the Hansen solubility parameters and the Hansen sphere radius with the aid of the solver add-in of Microsoft Excel," *SN Applied Sciences,* vol. 2, no. 4, 2020, doi: 10.1007/s42452-020-2512-y.

[30] L. Bergkamp and N. Herbatschek, "Regulating Chemical Substances under <scp>REACH</scp>: The Choice between Authorization and Restriction and the Case of Dipolar Aprotic Solvents," *Review of European, Comparative & International Environmental Law,* vol. 23, no. 2, pp. 221-245, 2014, doi: 10.1111/reel.12083.

[31] P. van de Witte, P. Dijkstra, J. Van den Berg, and J. Feijen, "Phase separation processes in polymer solutions in relation to membrane formation," *Journal of membrane science,* vol. 117, no. 1-2, pp. 1-31, 1996.
[32] J. Sherwood, T. J. Farmer, and J. H. Clark, "Catalyst: Possible Consequences of the N-Methyl Pyrrolidone REACH Restriction," *Chem,* vol. 4, no. 9, pp. 2010-2012, 2018, doi: 10.1016/j.chempr.2018.08.035.
[33] A. Bottino, G. Capannelli, S. Munari, and A. Turturro, "Solubility parameters of poly(vinylidene fluoride)," *Journal of Polymer Science Part B: Polymer Physics,* vol. 26, no. 4, pp. 785-794, 1988, doi: 10.1002/polb.1988.090260405.
[34] T. P. Knepper and F. T. Lange, *Polyfluorinated chemicals and transformation products*. Springer Science & Business Media, 2011.
[35] M. F. Rahman, S. Peldszus, and W. B. Anderson, "Behaviour and fate of perfluoroalkyl and polyfluoroalkyl substances (PFASs) in drinking water treatment: A review," *Water research,* vol. 50, pp. 318-340, 2014.
[36] S. A. Jacobs *et al.*, "Assessment of Fluoropolymer Production and Use With Analysis of Alternative Replacement Materials," United States, 2024. [Online]. Available: https://www.osti.gov/biblio/2370520

https://www.osti.gov/servlets/purl/2370520
[37] B. Van der Bruggen and C. Vandecasteele, "Modelling of the retention of uncharged molecules with nanofiltration," *Water research,* vol. 36, no. 5, pp. 1360-1368, 2002.
[38] F. Liu, N. A. Hashim, Y. Liu, M. R. M. Abed, and K. Li, "Progress in the production and modification of PVDF membranes," *Journal of Membrane Science,* vol. 375, no. 1-2, pp. 1-27, 2011, doi: 10.1016/j.memsci.2011.03.014.
[39] J.-H. Kim and K.-H. Lee, "Effect of PEG additive on membrane formation by phase inversion," *Journal of membrane science,* vol. 138, no. 2, pp. 153-163, 1998.
[40] D. Rana and T. Matsuura, "Surface modifications for antifouling membranes," *Chemical reviews,* vol. 110, no. 4, pp. 2448-2471, 2010.
[41] S. Azari, M. Karimi, and M. H. Kish, "Structural Properties of the Poly(acrylonitrile) Membrane Prepared with Different Cast Thicknesses," *Industrial & Engineering Chemistry Research,* vol. 49, no. 5, pp. 2442-2448, 2010/03/03 2010, doi: 10.1021/ie900952v.
[42] A. Ismail and A. Hassan, "Formation and characterization of asymmetric nanofiltration membrane: Effect of shear rate and polymer concentration," *Journal of Membrane Science,* vol. 270, no. 1-2, pp. 57-72, 2006.
[43] T.-S. Chung, J.-J. Qin, and J. Gu, "Effect of shear rate within the spinneret on morphology, separation performance and mechanical properties of ultrafiltration polyethersulfone hollow fiber membranes," *Chemical Engineering Science,* vol. 55, no. 6, pp. 1077-1091, 2000.
[44] A. F. Ismail, A. R. Hassan, and N. B. Cheer, "Effect of shear rate on the performance of nanofiltration membrane for water desalination," *Songklanakarin J. Sci. Technol,* vol. 24, pp. 879-889, 2002.
[45] B. S. Lalia, E. Guillen-Burrieza, H. A. Arafat, and R. Hashaikeh, "Fabrication and characterization of polyvinylidenefluoride-co-hexafluoropropylene (PVDF-HFP) electrospun membranes for direct contact membrane distillation," *Journal of membrane science,* vol. 428, pp. 104-115, 2013.

[46] M. C. García-Payo, M. Essalhi, and M. Khayet, "Effects of PVDF-HFP concentration on membrane distillation performance and structural morphology of hollow fiber membranes," *Journal of Membrane Science,* vol. 347, no. 1, pp. 209-219, 2010/02/01/ 2010, doi: https://doi.org/10.1016/j.memsci.2009.10.026.

[47] L. Lipsa, S. Rajput, S. Parida, S. P. Ghosh, S. K. Verma, and S. Gupta, "Influence of Hot-Press Temperature on β-Phase Formation and Electrical Properties of Solvent-Casted PVDF-HFP Co-Polymer Films Prepared from Two Different Solvents: A Comparison Study," *Macromolecular Chemistry and Physics,* vol. 224, no. 21, 2023, doi: 10.1002/macp.202300204.

[48] Z. Cui, N. T. Hassankiadeh, Y. Zhuang, E. Drioli, and Y. M. Lee, "Crystalline polymorphism in poly(vinylidenefluoride) membranes," *Progress in Polymer Science,* vol. 51, pp. 94-126, 2015, doi: 10.1016/j.progpolymsci.2015.07.007.

[49] R. Gregorio Jr, "Determination of the α, β, and γ crystalline phases of poly (vinylidene fluoride) films prepared at different conditions," *Journal of applied polymer science,* vol. 100, no. 4, pp. 3272-3279, 2006.

[50] K. Nakagawa and Y. Ishida, "Estimation of amorphous specific volume of poly(vinylidene fluoride) as a function of temperature," *Kolloid-Zeitschrift und Zeitschrift für Polymere,* vol. 251, no. 2, pp. 103-107, 1973, doi: 10.1007/bf01498933.

[51] D.-J. Lin, K. Beltsios, T.-H. Young, Y.-S. Jeng, and L.-P. Cheng, "Strong effect of precursor preparation on the morphology of semicrystalline phase inversion poly(vinylidene fluoride) membranes," *Journal of Membrane Science,* vol. 274, no. 1-2, pp. 64-72, 2006, doi: 10.1016/j.memsci.2005.07.043.

[52] T. Uragami, Y. Naito, and M. Sugihara, "Studies on synthesis and permeability of special polymer membranes," *Polymer Bulletin,* vol. 4, no. 10, 1981, doi: 10.1007/bf00256290.

[53] E. Fontananova, J. C. Jansen, A. Cristiano, E. Curcio, and E. Drioli, "Effect of additives in the casting solution on the formation of PVDF membranes," *Desalination,* vol. 192, no. 1-3, pp. 190-197, 2006, doi: 10.1016/j.desal.2005.09.021.

[54] S. P. Nunes and K. V. Peinemann, "Ultrafiltration membranes from PVDF/PMMA blends," *Journal of Membrane Science,* vol. 73, no. 1, pp. 25-35, 1992.

[55] M. Yeow, Y. Liu, and K. Li, "Morphological study of poly (vinylidene fluoride) asymmetric membranes: effects of the solvent, additive, and dope temperature," *Journal of Applied Polymer Science,* vol. 92, no. 3, pp. 1782-1789, 2004.

[56] A. Kumar, A. Sharma, B. G. De La Torre, and F. Albericio, "Scope and Limitations of γ-Valerolactone (GVL) as a Green Solvent to be Used with Base for Fmoc Removal in Solid Phase Peptide Synthesis," *Molecules,* vol. 24, no. 21, p. 4004, 2019, doi: 10.3390/molecules24214004.

[57] A. Kumar, A. Sharma, B. G. de la Torre, and F. Albericio, "Rhodiasolv PolarClean – a greener alternative in solid-phase peptide synthesis," *Green Chemistry Letters and Reviews,* vol. 14, no. 3, pp. 545-550, 2021, doi: 10.1080/17518253.2021.1965663.

[58] M. A. Rasool and I. Vankelecom, "Use of γ-valerolactone and glycerol derivatives as bio-based renewable solvents for membrane preparation," *Green chemistry,* vol. 21, no. 5, pp. 1054-1064, 2019.

[59] J. T. Jung, J. F. Kim, H. H. Wang, E. Di Nicolo, E. Drioli, and Y. M. Lee, "Understanding the non-solvent induced phase separation (NIPS) effect during the fabrication of microporous PVDF membranes via thermally induced phase separation (TIPS)," *Journal of Membrane Science,* vol. 514, pp. 250-263, 2016.

[60] N. T. Hassankiadeh *et al.*, "Microporous poly (vinylidene fluoride) hollow fiber membranes fabricated with PolarClean as water-soluble green diluent and additives," *Journal of Membrane Science,* vol. 479, pp. 204-212, 2015.

[61] F. Russo, C. Ursino, B. Sayinli, I. Koyuncu, F. Galiano, and A. Figoli, "Advancements in Sustainable PVDF Copolymer Membrane Preparation Using Rhodiasolv® PolarClean As an Alternative Eco-Friendly Solvent," *Clean Technologies,* vol. 3, no. 4, pp. 761-786, 2021, doi: 10.3390/cleantechnol3040045.

[62] G.-d. Kang and Y.-m. Cao, "Application and modification of poly(vinylidene fluoride) (PVDF) membranes – A review," *Journal of Membrane Science,* vol. 463, pp. 145-165, 2014, doi: 10.1016/j.memsci.2014.03.055.

[63] D. Lu, K. Jung, J. Y. Shim, T. A. L. Harris, and I. C. Escobar, "Manufacturing supported loose-nanofiltration polymeric membranes with eco-friendly solvents on an R2R System," *npj Clean Water,* vol. 7, no. 1, 2024, doi: 10.1038/s41545-024-00319-4.

[64] X. Dong, H. D. Shannon, C. Parker, S. De Jesus, and I. C. Escobar, "Comparison of two low-hazard organic solvents as individual and cosolvents for the fabrication of polysulfone membranes," *AIChE Journal,* vol. 66, no. 1, p. e16790, 2020.

[65] W. Xie *et al.*, "Using the Green Solvent Dimethyl Sulfoxide To Replace Traditional Solvents Partly and Fabricating PVC/PVC-g-PEGMA Blended Ultrafiltration Membranes with High Permeability and Rejection," *Industrial & Engineering Chemistry Research,* vol. 58, no. 16, pp. 6413-6423, 2019/04/24 2019, doi: 10.1021/acs.iecr.9b00370.

[66] X. Dong, H. D. Shannon, and I. C. Escobar, "Investigation of polarclean and gamma-valerolactone as solvents for polysulfone membrane fabrication," in *Green Polymer Chemistry: New Products, Processes, and Applications*: ACS Publications, 2018, pp. 385-403.

[67] N. Ali, N. S. Halim, A. Jusoh, and A. Endut, "The formation and characterisation of an asymmetric nanofiltration membrane for ammonia-nitrogen removal: effect of shear rate," *Bioresour Technol,* vol. 101, no. 5, pp. 1459-65, Mar 2010, doi: 10.1016/j.biortech.2009.08.070.

[68] M. V. X. Klaus, A. M. Gutierrez, and J. Z. Hilt, "Development of Poly(acrylamide)-Based Hydrogel Composites with Powdered Activated Carbon for Controlled Sorption of PFOA and PFOS in Aqueous Systems," *Polymers,* vol. 15, no. 22, p. 4384, 2023, doi: 10.3390/polym15224384.

[69] S. S. Sreedhara and N. R. Tata, "A novel method for measurement of porosity in nanofiber mat using pycnometer in filtration," *Journal of Engineered Fibers and Fabrics,* vol. 8, no. 4, p. 155892501300800408, 2013.

[70] Z. Guo, R. Xiu, S. Lu, X. Xu, S. Yang, and Y. Xiang, "Submicro-pore containing poly (ether sulfones)/polyvinylpyrrolidone membranes for high-temperature fuel cell applications," *Journal of Materials Chemistry A,* vol. 3, no. 16, pp. 8847-8854, 2015.

[71] N. Uguen, "Dispersion state, interfacial phenomena and dielectric properties in high-permittivity polymer-based nanocomposites

Effet de l'état de dispersion et de la modification de surface de particules à haute permittivité sur les propriétés diélectriques de nanocomposites à base polymère," Université de Lyon, 2022LYSE1032, 2022. [Online]. Available: https://theses.hal.science/tel-04008532

[72] X. Dong, A. Al-Jumaily, and I. C. Escobar, "Investigation of the use of a bio-derived solvent for non-solvent-induced phase separation (NIPS) fabrication of polysulfone membranes," *Membranes,* vol. 8, no. 2, p. 23, 2018.

[73] A. Henni, J. J. Hromek, P. Tontiwachwuthikul, and A. Chakma, "Volumetric Properties and Viscosities for Aqueous N-Methyl-2-pyrrolidone Solutions from 25 °C to 70 °C," *Journal of Chemical & Engineering Data,* vol. 49, no. 2, pp. 231-234, 2004, doi: 10.1021/je034073k.

[74] A. Fionah *et al.*, "Microcystin-LR removal from water via enzymatic linearization and ultrafiltration," *Toxins,* vol. 14, no. 4, p. 231, 2022.

[75] N. M. Ghasem, M. H. Al-Marzouqi, and M. H. El-Naas, "Effect of temperature, composition, and shear rate on polyvinylidene fluoride/dimethylacetamide solution viscosity," *Journal of Chemical & Engineering Data,* vol. 54, no. 12, pp. 3276-3280, 2009.

[76] F. Sadeghi, S. Tabatabaei, P. Carreau, and A. Ajji, "Structure and properties of MDO stretched films of a random co-polypropylene and a linear polypropylene blend," *Annual Technical Conference - ANTEC, Conference Proceedings,* vol. 4, pp. 2328-2331, 01/01 2009.

[77] X. Wang, C. Xiao, H. Liu, Q. Huang, and H. Fu, "Fabrication and properties of PVDF and PVDF-HFP microfiltration membranes," *Journal of Applied Polymer Science,* vol. 135, no. 40, p. 46711, 2018, doi: 10.1002/app.46711.

[78] A. Jabbarnia and R. Asmatulu, "Synthesis and Characterization of PVdF/PVP-Based Electrospun Membranes as Separators for Supercapacitor Applications," *Journal of Material Science and Technology Research,* vol. 2, no. 2, pp. 43-51, 2021, doi: 10.15377/2410-4701.2015.02.02.3.

VITA

1. University of Kentucky, Bachelor of Science in Chemical Engineering, Minor in Flute Performance
2. Undergraduate Research Assistance, University of Kentucky Center for Applied Energy Research, Graduate Research Assistant, University of Kentucky Membrane Science Center
3. University of Kentucky Superfund Research Center Trainee, University of Kentucky National Research Traineeship Trainee
4. Cakmak, E., Hower, J. C., Mathews, J. P., Weisenberger, M. C., Kaplan, R., Lacy, J., Zhang, Y., & Lara-Curzio, E. (2023). Microstructural diversity and digestion yields of select bituminous and subbituminous coals as raw material candidates for carbon fiber precursor production. *Fuel*, *348*, 128545. https://doi.org/https://doi.org/10.1016/j.fuel.2023.128545
5. Rachel Kaplan